Okinawa Institute of Science and Technology
Graduate University

Thesis submitted for the degree
Doctor of Philosophy

Effects of Mean Flow and Turbulence on Planktivory by Anchored Garden Eels and Site-Attached Fish

by
Kota Ishikawa

Supervisor: Satoshi Mitarai
Co-supervisor: Amatzia Genin
Hebrew University of Jerusalem

February, 2024

Declaration of Original and Sole Authorship

I, Kota Ishikawa, declare that this thesis entitled *Effects of mean flow and turbulence on planktivory by anchored garden eels and site-attached fish* and the data presented in it are original and my own work.

I confirm that:

- No part of this work has previously been submitted for a degree at this or any other university.
- References to the work of others have been clearly acknowledged. Quotations from the work of others have been clearly indicated and attributed to them.
- In cases where others have contributed to part of this work, such contribution has been clearly acknowledged and distinguished from my own work.
- None of this work has been previously published and pre-printed elsewhere, with the exception of the following:

  Ishikawa, K., Wu, H., Mitarai, S., and Genin, A. (2022) Effects of prey density and flow speed on plankton feeding by garden eels: A flume study. J. Exp. Biol. 225, 1–10. doi:10.1242/jeb.243655.
  (Contribution: I conceived the study with A.G. I designed the methods and analysis with co-authors. I performed flume experiments and field observation with contributions from H.W. for PIV measurements. I analyzed the data with help from H.W. I wrote the original draft. All authors discussed the results and commented on the manuscript.)

Date: **February 8th, 2024**

Signature: 

Abstract

Water flow is a key environmental factor that affects fish in coral reefs. Changes in flow properties, such as mean flow speed and turbulent fluctuation, have been expected to affect the feeding of zooplanktivorous fish through its effects on the motions of both prey and predator. Flows are critical not only for freely swimming fish but also for anchored fish, such as garden eels, that feed while anchored to the sandy bottom by keeping the posterior parts of their bodies inside a burrow.

The objective of this study is to comparatively examine effects of flows on freely swimming reef fish and anchored garden eels to understand ecological traits, such as adaptation, habitat selection, and prey-predator interaction. To address this objective, I combined flow measurements in the field and flume experiments designed to examine effects of mean flow speed and small-scale turbulence on feeding and energy cost of reef damselfish (*Chromis viridis*) and garden eels (*Heteroconger hassi*). In situ flow measurements by acoustic Doppler velocimeter (ADV) indicated faster flow speed and stronger turbulence at damselfish habitat above corals compared with garden eel habitat on a flat sandy bottom. Based on the in situ flow measurement, a range of mean flow speed and small-scale turbulence in dissipation range was reproduced in flumes to examine fish responses by label-free tracking of body points and 3D movement analysis. The relationship between feeding rate and flow speed showed an adaptation of damselfish to faster flow speed compared to garden eels. The energy cost and benefit model also indicated that the energetically optimal range of flow speed of damselfish was faster than that of garden eels. Detailed motion analysis revealed a unique strategy of garden eels to flow speed, leading to the development of first foraging model for this group of fish. The anchored and site-attached fish also differed in their responses to small-scale turbulence: strong turbulence caused a decrease in feeding rates under slow flows for damselfish and under fast flows for garden eels. The turbulence effect was associated with a reduction of the foraging area for damselfish and an increase of the search time for garden eels. By combining field flow measurements and flume experiments, my study advanced the understanding of adaptations to hydrodynamic conditions in fish.

Acknowledgements

I would like to express my sincere gratitude to my supervisor, Satoshi Mitarai, and my co-supervisor, Amatzia Genin for their support and guidance throughout my thesis research. Their critical advice from diverse perspectives played a pivotal role in shaping and enhancing the quality of this interdisciplinary study. Special thanks go to Heng Wu, a post-doc in our unit, for providing her knowledge and skills in programming and fluid dynamics. Her support on a daily basis significantly contributed to my learning curve in these unfamiliar fields and turned me into a researcher with interdisciplinary skills. Discussions with these three remarkable researchers always provided inspiration and different ways of thinking.

I extend my appreciation to the funding sources that made this research possible— the Okinawa Institute of Science and Technology's high-trust fund and the Japan Society for the Promotion of Science DC2 fellowship (JSPS KAKENHI JP23KJ2133). I am grateful to both former and current unit members, with a special acknowledgement to Otis Brunner for providing guidance to Ph.D. life, Po-Shun Chuang (Bob) for insightful research discussions, Akinori Murata for technical support for fieldworks, and Kazumi Inoha and Tomoko Yoshino for their administrative support. I also appreciate OIST Engineering Section and Marine Science Section for generous support. I thank Irena Kolesnikova for making a plankton net, Stefano Olivieri for advice on grid geometry, and Yoshikatsu Nakano, Kim Chanyoung, Yoshitaka Zukeyama, Yutaka Yonamine, and Takuma Toyama for technical support of field work.

I greatly appreciate my thesis committee, Samuel Reiter and Akihiro Kusumi for their input and feedback. I am also grateful to my proposal examiners, Peter Wainwright and Noriyuki Satoh for their insightful suggestions that greatly contributed to refining the proposed research. Special mention goes to Alexandra Khrizman for sharing her expertise and knowledge obtained from her master's research on garden eels in the Red Sea. Lastly, I would like to thank my former supervisor Takashi Kato and the members of his lab for imparting the foundation of scientific approach and theoretical thinking upon which I built my thesis research.

List of Abbreviations

ADV	-Acoustic Doppler Velocimetry
ANOVA	-Analysis of Variance
BCF	-Body-Caudal Fin
DBA	-Dynamic Body Acceleration
DLT	-Direct Linear Transformation
DLW	-Doubly Labeled Water
DW	-Dry Weight
FBF	-Fin Beat Frequency
GLMM	-Generalized Linear Mixed Model
MPF	-Median-Paired Fin
PIV	-Particle Image Velocimetry
PSD	-Power Spectral Density
REML	-Restricted Maximum Likelihood
SMR	-Standard Metabolic Rate
TKE	-Turbulence Kinetic Energy
VeDBA	-Vectorial Dynamic Body Acceleration

List of Publication

- Ishikawa, K., Wu, H., Mitarai, S., and Genin, A. (2022) Effects of prey density and flow speed on plankton feeding by garden eels: A flume study. J. Exp. Biol. 225, 1–10. doi:10.1242/jeb.243655.
  Contribution: I conceived the study with A.G. I designed the methods and analysis with co-authors. I performed flume experiments and field observation with contributions from H.W. for PIV measurements. I analyzed the data with help from H.W. I wrote the original draft. All authors discussed the results and commented on the manuscript.

Table of Contents

List of Figures and Tables

Introduction

Plankton-feeding fish (planktivorous fish) play an important role in material transport in coral reefs. Planktivorous fish decrease zooplankton extensively in reefs and digest it into feces, contributing to the movement of carbon, nitrogen, and nutrients (Hamner et al., 1988). To understand abundance, distribution, and ecological interactions of these fish, it is essential to reveal their behavioral responses to environments. Feeding behavior, in particular, has been studied extensively because that is how fish acquire energy for growth and reproduction. Zooplankton feeding by fish depends on various biotic factors, such as prey density (Kiflawi and Genin, 1997; Noda et al., 1992), prey size (Hill and Grossman, 1993; Manatunge and Asaeda, 1998), and risk of predation (Morgan, 1988), as well as abiotic factors, such as currents (Clarke et al., 2009; Finelli et al., 2009; Fulton et al., 2005a; Kiflawi and Genin, 1997), light (Howard and Bori, 1972; Manatunge and Asaeda, 1998; Rickel and Genin, 2005), and water temperature (Nilsson et al., 2010).

Among these factors, flows heavily influence fish foraging and other behaviors. For example, some fish alter their behavior in response to changes in flows by adjusting their strike distance and lateral angle, by changing proportions of fin type usage, or by adopting sheltering behavior (Heatwole and Fulton, 2013; Johansen et al., 2008a; Kiflawi and Genin, 1997). Because of the significant effects of flows on fish feeding, foraging models have been developed by involving flows as a main environmental factor. Models for drift-feeding river fish and coral reef fish rely on a wedge-shaped area affected by the fish's reaction distance and angle, both of which depend on flow speed. (Fausch, 1984; Kiflawi and Genin, 1997). Also, efficiency of prey detection is largely affected by flows and included in models (Piccolo et al., 2014). According to these foraging models and experimental data, the feeding rate of planktivorous reef fish show a dome-shaped curve against flow speed, where it initially increases at a decreasing rate, reaches a maximum, and declines as flow speed increases (Clarke et al., 2009; Kiflawi and Genin, 1997). The foraging models have been useful in predicting ecological traits, such as adaptation, habitat selection, and predator-prey interactions (Kiflawi and Genin, 1997; Piccolo et al., 2014; Rosenfeld and Boss, 2001).

Fish acquire energy by feeding, but at the same time, fish must expend energy for feeding and other activities. To succeed and survive through natural selection, fish select locations where they can maximize net energy gain (Fausch, 1984; Hill and Grossman, 1993; Piccolo et al., 2014), defined as energy intake by feeding minus the cost of swimming; thus, net energy is available for growth and reproduction. Therefore, it is important to understand energy cost of locomotion and activities in addition to energy gain by feeding. Energy cost of fish is largely affected by flow speed. For example, energy expenditure of fish in rivers and oceans during locomotion usually increases as flow speed increases (Asaeda et al., 2005; Fausch, 1984; Marcoux and Korsmeyer, 2019). Also, responses of energy costs to flows depend on morphological and functional traits, such as body shape, fin shape, and locomotion modes (Korsmeyer et al., 2002; Marcoux and Korsmeyer, 2019; Schakmann and Korsmeyer, 2023).

By assessing net energy gain as a function of environmental parameters, energy-based cost-benefit models have been developed to explain optimal environments for fish and have been used to predict fish distributions and abundance and to assess habitat quality (Piccolo et al., 2014). These models are mainly for drift-feeding river fish and use flows as an environmental parameter because flows strongly affect both feeding and swimming costs of station-holding fish. However, to the author’s knowledge, no empirical studies have comprehensively assessed energy costs and benefits for fish in coral reefs although water motion affects habitat distribution and reef fish community structure through its effects on fish morphology and behavior (Binning and Roche, 2015; Depczynski and

Bellwood, 2005; Fulton and Bellwood, 2005). Because coral reef fish are usually site-attached rather than free-ranging, cost-benefit models focused on flow speed should be useful to understand adaptation and habitat selection.

One of the limitations of the cost-benefit models is that energy cost is usually measured via oxygen consumption in a respirometer during steady swimming. Feeding and other activities often involve rapid changes in speed and direction and in turn, cost more than steady behavior (Bidder et al., 2017). However, small chambers used for standard respirometry methods do not allow fish to keep the full range of reactive distance to prey during feeding (Kiflawi and Genin, 1997). Other than respirometry, there are various methods to quantify energy cost of fish. In laboratories, another common method is direct calorimetry, which measures heat production from animals (Kenny et al., 2017; Lusk, 1932), but this method also requires fish in a small chamber where fish cannot show normal feeding behavior. In the field, heart rate method which uses heart beat as a proxy of energy cost based on calibration curves made in laboratories (Butler et al., 2004; Speakman and Racey, 1988), but it is invasive because of an implanted logger. Another relatively new method uses dynamic body acceleration (DBA; acceleration from animal movement) as a proxy of energy cost (Wilson et al., 2006). DBA has been proven to have a high correlation with oxygen consumption during active behaviors in a wide range of animal taxa (Halsey et al., 2009; Halsey et al., 2011; Lyons et al., 2013; Payne et al., 2011; Robson et al., 2012; Wilson et al., 2020). However, a logger attachment makes it impractical to apply this method to small animals, such as planktivorous fish that are less than few hundreds grams (Brownscombe et al., 2018; Gleiss et al., 2010; Lear et al., 2016; Metcalfe et al., 2016; Noda et al., 2016; Robson et al., 2012). Thus, new methods that enables energy cost estimation during feeding of small fish are necessary to improve cost-benefit models.

The foregoing research on effects of flows on fish behavior was focused primarily on effects of mean flow speed (time-averaged streamwise flow speed usually measured at the center of a test section to avoid effects of boundary layers). The uniform flows produced in laboratory settings may not represent complex flows in the natural habitats of fish. In an attempt to reproduce flows that fish experience in natural habitats, effects of more complex flows have also been investigated (Higham et al., 2015; Liao, 2007; Trinci et al., 2017). Fish exploit flows around cylindrical structures mainly by reducing body movement and swimming at low velocity in front of a cylinder (bow-waking), angling the body into the mean flow direction (entraining), and synchronizing body rhythm with the Karman vortex street behind the cylinder (karman-gaiting; Liao 2007). On the other hand, complex flows alter fin beating, reduce swimming speed, induce destabilization, and enhance oxygen consumption (Lupandin, 2005; Maia et al., 2015; Roche et al., 2014). Notably, some studies report a negligible effect of complex flow on fish swimming performance (Nikora et al., 2003).

These fish locomotion studies used wake flows produced by cylindrical structures, turbines, and specific wall shapes. However, especially for foraging studies, mimicking turbulence with more stochasticity is important because fish may learn predictable prey movements in wake flows. To avoid flows in flumes being dominated by a specific frequency, grid-generated turbulence was used to study its effect on oxygen consumption of shiner perch (van der Hoop et al., 2018). The fish decreased oxygen consumption under stronger turbulence, but the mechanism of reduced energy expenditure was unclear. Moreover, previous studies on effects of complex flows mainly focused on fish locomotion or movement. However, as complex flow is expected to affect both prey movement and fish behavior, its effect on feeding warrants further investigation (Clarke et al., 2009).

When studying effects of turbulence on aquatic animals in the laboratory, the ecological relevance of turbulence levels is often validated by citing other studies that measured turbulence in an environment where the subject species is likely to live. However, turbulence levels in the laboratory may not represent those experienced by aquatic animals (Franks et al., 2022; Peters and Redondo, 1997). Also, in some cases, it is unclear whether the species used in laboratory experiments exists in field sites.

As described above, there have been extensive studies on effects of flows on fish that swim freely while foraging for zooplankton in seas, lakes, and rivers, yet few studies have addressed stationary fish that feed while anchored to the bottom. One example of 'anchored' fish is garden eels that live in sandy areas around coral reefs and feed on zooplankton while burying a part of their bodies in the sand (Smith, 1989). The eel's posterior body remains buried in the sand during foraging, serving as an anchor. Thirty-six species of garden eel have been found in the tropics worldwide (Fricke et al., 2021). Because their movements are limited by their burrows that they rarely change (Smith, 1989), it is critical to understand environmental effects on their behavior. A recent field study examined feeding dynamics of one species of garden eel (*Gorgasia sillneri*) in the Red Sea and found that their unique body posture under fast flow speed reduces drag imposed on the eels (Khrizman et al., 2018). They also found that the species showed a monotonic increase in feeding rate with flow speed, as well as with prey density, which is exceptional as a planktivorous fish. However, it is challenging to isolate effects of one environmental parameter from others in in situ observations. Also, energy cost of this type of fish is yet to be known because it is difficult to measure small oxygen consumption from the fish as the signal is interrupted by bacterial respiration from a large amount of sand.

Research Objectives

The goal of this study is to understand effects of mean flow speeds and turbulent fluctuations on feeding and energy balance planktivorous fish in coral reefs by combining flow measurement in fish habitats and flume experiments and by comparing site-attached free fish and anchored garden eels.

In Chapter 1, I focused on anchored fish and investigated their feeding responses to flow speed and prey density in a custom-made flume. Using spotted garden eels (*Heteroconger hassi*), feeding rates and detailed behavior during feeding were measured with label-free tracking and 3D movement analysis. Based on the analysis, a foraging model using the body length extended from the burrow was developed. The results and comparison with previous findings on site-attached fish suggest that due to their unique foraging mode, garden eels can occupy self-made burrows in exposed shelter-free sandy bottoms where they can effectively feed on drifting zooplankton.

In Chapter 2, I compared cost-benefit models of site-attached fish and anchored garden eels. To estimate energy cost of fish during feeding, I used 3D DBA measured by tracking marker-less body points in videos and reconstructing them into 3D. The video-based DBA of damselfish was shown to have high correlations with oxygen consumption rates measured in a respirometer, suggesting that it is a good proxy of energy expenditure. Together with the quantification of oxygen consumption during steady swimming and feeding and that of energy gain estimated by feeding rates, I developed quantitative cost-benefit models of site-attached free fish. Also, using DBA and feeding rates during feeding behavior, changes in energy cost and gain of garden eels under different flow speeds were estimated. Based on the cost-benefit models of the two species, the energetically efficient flow speed range was identified and compared with flow speeds in their habitats.

In Chapter 3, I investigated effects of grid-generated turbulence on zooplanktivory by site-attached free damselfish and anchored garden eels by combining field flow

measurements and controlled flume experiments. Under different turbulence levels, feeding rates and 3D feeding movements were examined. The two types of fish responded very differently to small-scale turbulence. The causes of the difference are discussed in relation to environments in each habitat.

Assessment of effects of flows on feeding kinematics and energy cost-benefit is essential to understand adaptation, habitat distribution, and ecological interactions in changing environments. This study sought to understand effects of mean flow speed and small-scale turbulent fluctuations on foraging and energy cost-benefit with fine resolution in experimental flumes. Subject species included not only site-attached free fish in coral reefs but also stationary garden eels. By revealing how flows affect feeding behavior of site-attached free damselfish and anchored garden eels, this study will better understand how each species feeds while adapting to changes in mean flow speed and turbulent fluctuation. Detailed analysis of foraging movement will reveal strategies for survival and adaptation. A cost-benefit model will enable estimations of habitat distribution. In summary, my thesis research will advance our knowledge of the behavioral ecology of reef fish feeding in flows.

Chapter 1

Effects of Mean Flow Speed on Planktivory by Anchored Garden Eels

1.1. Introduction

Understanding of environmental effects on feeding kinematics of planktivorous fish has been largely limited to free fish that can swim freely to capture prey. Few studies have addressed foraging of stationary fish that feed while anchored to substrates. Garden eels are one of the anchored fish that inhabit sandy areas around coral reefs (Smith, 1989). Their distinctive feeding method involves capturing zooplankton while burying their posterior parts of their body in the sand (Smith, 1989). This unique and limited way of feeding makes it essential to understand environmental effects on their behavior. Although there is one field study that examined feeding of one species of garden eels in the Red Sea (Khrizman et al., 2018), precise measurements of feeding rates and behavioral analysis in a laboratory flume were required to resolve effects of flow speed and other environmental factors finely.

1.2. Published Article

Ishikawa, K., Wu, H., Mitarai, S., and Genin, A. (2022) Effects of prey density and flow speed on plankton feeding by garden eels: A flume study. *J. Exp. Biol*. **225**, 1–10. doi:10.1242/jeb.243655.

1.3. Chapter Conclusion

In this chapter, using a custom-made flume with a sandy bottom, I quantified the isolated effects of mean flow speed on feeding rates by spotted garden eels (*Heteroconger hassi*). Contrary to the field study (Khrizman et al., 2018), garden eels in this study showed a decrease in feeding rates at a flow speed of 25 cm s^{-1}. With label-free tracking of body points and three-dimensional movement analysis, I found that the reduction in feeding rate at faster flow speed resulted from modulation of the eel's movements (shorter exposure and bending), which helped eels to inhibit the expected increase of drag. Also, a foraging model based on the body length extended from the burrow was developed, showing correspondence with observations. These findings demonstrate their unique strategy to adapt to live in relatively exposed sandy areas with reduced competition from other planktivorous fish.

Chapter 2

Effects of Mean Flow Speed on Energy Cost and Benefit of Site-Attached Fish and Anchored Garden Eels

2.1. Introduction

Fish acquire energy by feeding and consume a part of it by various activities, particularly movements. The remaining energy gained is the net energy gain. To succeed and survive through natural selection, it is important for fish to maximize net energy gain which is energy mainly used for growth and reproduction. The quantification of the net energy gain of fish species has led to the development of species-specific cost-benefit models. Many cost-benefit models have been developed to estimate habitat selection of drift-feeding river fish. Drift-feeding is a feeding strategy used for fish in flowing water, in which fish face upstream to capture drifting prey. This feeding strategy results in energy optimization, as fish select habitats to maximize energy gain and minimize energy expenditure (Hill and Grossman, 1993; Piccolo et al., 2014). In these models, flow speed is the dominant parameter because it affects both drifting prey flux and swimming cost. Since Fausch (1984) developed the first quantitative energy cost-benefit model, many models have been established and tested for habitat selection (reviewed in Piccolo et al., 2014).

In coral reefs, water motion drives species distribution and community structure through its effects on behavior and morphology (Binning and Roche, 2015; Fulton and Bellwood, 2005; Fulton et al., 2005b; Korsmeyer et al., 2002). These morphological and functional traits are thought to represent adaptations to flows. For example, body-caudal fin (BCF) swimmers use lateral undulation of body and caudal fin to create thrust, which provides greater power for sustained swimming in fast flows, whereas median-paired fin (MPF) swimmers use median or paired fin propulsion, which provides better maneuverability in complex environments (Blake, 2004; Webb, 1984). Although most fish are BCF swimmers, more than 60% of fish in coral reefs are pectoral fin swimmers (Fulton and Bellwood, 2005), reflecting the complex geometry and flow regimes in coral reefs. To understand how these morphological and functional differences help fish energetically to live in different flow environments, comparative studies have examined oxygen consumption of fish with different swimming modes and morphology and have provided significant understanding of suitable habitats for different types of fish (Korsmeyer et al., 2002; Marcoux and Korsmeyer, 2019; Schakmann and Korsmeyer, 2023). As highlighted in Chapter 1, however, flows also affect prey flux and foraging of fish in coral reefs (Clarke et al., 2009; Ishikawa et al., 2022; Kiflawi and Genin, 1997); hence, examining both energy gain and expenditure is important to understand adaptation and habitat selection.

Estimation of energy gain can be done relatively easily by measuring prey ingestion rate. However, quantifying energy cost of small planktivorous fish, especially during feeding, is challenging because of the limitations of the methods currently available. There are various methods to quantify energy cost of animals. In laboratories, common methods are direct calorimetry which measures heat production from animals (Kenny et al., 2017; Lusk, 1932) and indirect calorimetry which estimates energy expenditure by measuring oxygen consumption by animals (Frappell et al., 1989; Mtaweh et al., 2018). In field, standard methods are doubly labeled water (DLW) method which measures CO_2 production by using different elimination rates of stable isotopes or heart rate method which uses heart beat as a proxy of energy cost based on calibration curves made in

laboratories (Butler et al., 2004; Speakman and Racey, 1988). Each method has limitations, such that laboratory methods being confined by small chambers, DLW method being limited by low temporal resolution, and heart rate method being invasive because of an implanted logger. To understand energy cost of planktivorous fish feeding, it requires a larger volume than the chambers used for calorimetry methods in laboratory, finer temporal resolution than DLW method, and an impractically small logger for heart rate method.

An effective method that uses dynamic body acceleration (DBA) as a proxy of energy cost was developed in 2006 (Wilson et al., 2006). The basis of the DBA method is the fact that major part of energy consumption of animals is related to movement (Gleiss et al., 2011; Halsey et al., 2009). To measure DBA, animals are tagged with a logger including a tri-axial accelerometer. DBA has been proved to have a high correlation with oxygen consumption during active behaviors in a wide range of animal taxa, covering all five classes of vertebrates and some invertebrates (Halsey et al., 2009; Halsey et al., 2011; Lyons et al., 2013; Payne et al., 2011; Robson et al., 2012; Wilson et al., 2020). The correlations were valid even for fish species, such as sharks and sea bass, swimming steadily in a flume (Gleiss et al., 2010; Wright et al., 2014). Because of its technical simplicity and generality of the correlation with oxygen consumption, the method has been rapidly applied across a range of fields, leading to key biological findings, such as optimized foraging strategy of pumas (Williams et al., 2014), flight cost dependent survival of juvenile birds (Rotics et al., 2016), and energy cost related breeding performance of penguins (Grémillet et al., 2018). However, because the DBA method requires attachment of a logger that involves an accelerometer, battery, and memory, animals need to be large enough to ensure negligible effects of the logger on their behavior (Metcalfe et al., 2016). Many studies have used loggers less than 2–4% of the animals body weight (Halsey et al., 2009; Wilson et al., 2020). Given that loggers used for the DBA method are often 10–20 g (Brownscombe et al., 2018; Gleiss et al., 2010; Lear et al., 2016; Metcalfe et al., 2016; Noda et al., 2016; Robson et al., 2012), body weight of animals should be at least few hundreds of grams. Therefore, energy cost of foraging small planktivorous reef fish cannot be measured properly by the current DBA method that requires tag attachment.

In this chapter, the goal was to develop cost-benefit models of site-attached damselfish and anchored garden eels. To understand energy cost during feeding, I first developed a method to estimate oxygen consumption rate of damselfish. I measured 3D DBA by tracking marker-less body points in videos and reconstructing them into 3D and examined correlations between the DBA and oxygen consumption rate measured in a respirometer. Using small damselfish (*Chromis viridis*; <10 g), I demonstrated that video-based DBA is a good proxy of oxygen consumption rates. With the calibration curves obtained in the respirometer, oxygen consumption rates during foraging in a bigger flume were estimated. Also, relative energy cost of garden eels in response to changes in flow speed was estimated using the same method. By combining energy cost estimated by oxygen consumption rates or DBA and energy gain estimated by feeding rates, I developed cost-benefit models of free fish and anchored fish. The flow speed ranges where fish can effectively gain the net energy was obtained from the cost-benefit models and discussed in relation to flow speed range measured in their habitats.

2.2. Methods

Flow measurements in the field

To understand mean flow speed in the fish habitats, field observations were conducted in the habitats of the subject species, spotted garden eels (hereafter "garden eels"; *Heteroconger hassi*; Klausewitz and Eibl-Eibesfeldt 1959) and blue-green chromis (hereafter "chromis"; *Chromis viridis*; Cuvier 1830) in Onna, Okinawa, Japan (Figure 2.1). The habitat of chromis is about 3 m deep, with many patches of rocks and corals (patch reefs) dominated by *Acropora* corals which provide shelter (26°30'27N; 127°51'23"E; site A). In contrast, garden eels inhabit water about 16 m deep, with a sandy bottom and scattered patches of rocks and corals (26°30'39"N; 127°52'44"E; site B). In the area of these habitats, a maximum range of tides was approximately 2 m. An acoustic Doppler velocimeter (ADV, Vector, Nortek) was deployed from 27th September–27th October at site A and 14th July–14th August at site B in 2022. Measured volume was ~50 cm from a patch reef (220 cm from the bottom) for site A and 60 cm from a sandy bottom for site B. Every 30 min, the ADV initiated a 10-min measurement burst that measured velocities at 32 Hz. Velocity data were screened for low-beam correlations (<60%). Mean flow speed was computed by averaging flow velocities along all three axes for each 10-min burst (Gross and Nowell, 1983).

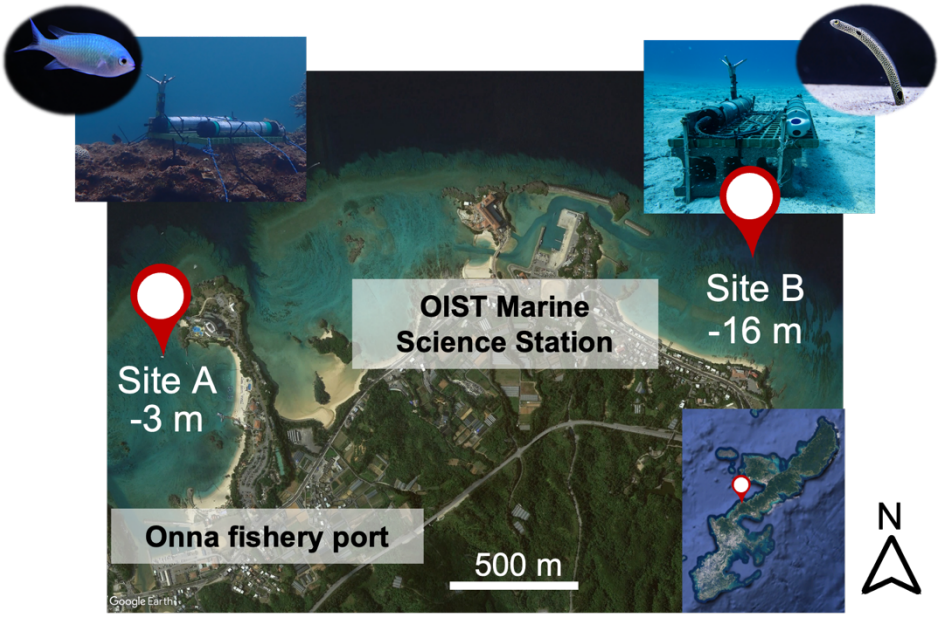

Figure 2.1. Site map of the Onna coast, Okinawa, indicating the locations of habitats where damselfish (site A) and garden eels (site B) are found. The map imagery is from Google Earth Pro.

Laboratory experiments

To understand energy cost and gain of chromis, oxygen consumption rates and feeding rates were measured in a respirometer and a bigger flume, respectively. To further understand energy cost of chromis during foraging, correlation between oxygen consumption rate and vectorial dynamic body acceleration (VeDBA) was examined. Using the calibration curves, oxygen consumption rate during foraging was estimated. For garden eels, feeding rates and VeDBA during foraging were extracted from Ishikawa et al. (2022).

Chromis were purchased from Aqua Planning Co., Ltd. This species distributes widely in the Indo-Pacific Ocean and is common in Okinawa. Five chromis, designated A to E, with

body weights of 6.59, 6.58, 5.17, 8.87, and 9.32 g respectively, were used in experiments. Except for these experiments, fish were kept in a holding tank and fed with brine shrimp (*Artemia salina*) nauplii, 0.59±0.05 mm (mean±SD, *n*=60) in length *ad libitum*. All experiments were conducted with approval from the Animal Care and Use Committee at Okinawa Institute of Science and Technology Graduate University.

Oxygen consumption measurements

Because of the difficulties to measure oxygen consumption of eels with a large amount of sand needed, oxygen consumption measurements were made only for chromis. Oxygen consumption experiments were conducted in a 10-L recirculating swimming respirometer (Loligo® Systems) with a test section 38 cm long, 10 cm wide, and 10 cm deep (Figure 2.2). A flow straightener was placed at the inlet of the test section to eliminate secondary flow. Flow in the respirometer was driven by an impeller. Using particle image velocimetry (PIV; detailed description of the system in Chapter 3), the frequency of the impeller and streamwise mean flow speeds at the center of the test section (averaged over a small area of 0.93×0.93 cm) were calibrated from 0 to 49.6 cm s^{-1}. The entire respirometer was immersed in a water bath to maintain the water temperature at 25.5±0.5°C. A light (Mitras lightbar 60, GHL, Germany) was placed above the center of the test section to provide illumination between 07:00 h and 19:00 h (12 h:12 h light:dark).

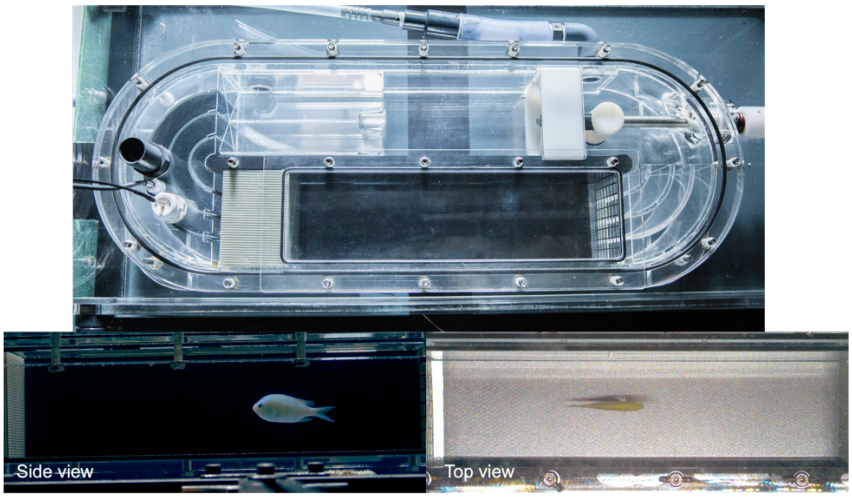

Figure 2.2. Recirculating swimming respirometer and images of fish during experiments.

To acquire a range of DBA values, six mean flow speeds were chosen based on the field measurement, and their effects were examined for five individuals of chromis. Two replicates were carried out for each individual at each flow speed (total N=60).

Individual fish were transferred into a respirometer the night before measurements and were kept at a mean flow speed of 5 cm s^{-1} overnight (13-15 h) for acclimation. After the acclimation period and after confirming that the oxygen concentration was stable and that the fish showed normal swimming behavior, a trial was started. Each trial comprised a series of twelve measurement cycles at increasing flow speeds from 5 to 30 cm s^{-1} at increments of 5 cm s^{-1} and two measurements at each flow speed. Each measurement cycle consisted of 5 min of flush, 2 min of equilibration, and 20 min of measurement following intermittent flow respirometer protocols (Steffensen, 1989; Steffensen et al., 1984). After each trial, fish were removed from the respirometer and their body weights were measured. Oxygen concentration was measured by the dipping probe oxygen mini sensor (Loligo® Systems), and temperature was measured by the temperature probe for witrox (Loligo®

Systems) with WitroxView software (Loligo® Systems). To inhibit bacterial growth, the whole tank was treated with bleach solution a day before each trial. Background respiration without fish was measured before and after a trial and the averaged respiration rate was subtracted from the respiration rate of trials with fish to obtain respiration rate from fish.

Based on the last 15 min of measurement for each cycle, linear regression was conducted between oxygen concentration (mg O_2 L^{-1}) and time (h). Using the slope of the linear regression, *S*, oxygen consumption rate, $\dot{M}O_2$ (mg O_2 kg^{-1} h^{-1}) was computed as

$$\dot{M}O_2 = SV_{resp}M^{-1}, \quad (2.1)$$

where V_{resp} is the volume of the respirometer, and *M* is the mass of the fish. In this study, $\dot{M}O_2$ was defined as the oxygen consumption rate scaled by fish weight. The fish behavior during the 15 min was recorded by cameras to obtain DBA, details of which are described below.

Oxygen consumption rates of five individuals were then plotted against the mean flow speed, *U*, and fitted with a three-parameter power function using the nonlinear least squares method ($\dot{M}O_2 = a + bU^c$; Roche et al., 2013). From the nonlinear relationship, standard metabolic rate (SMR) which is the minimal amount of energy required for maintenance or resting metabolic rate was estimated by extrapolation ($\dot{M}O_2$ at $U = 0$; Roche et al., 2013). The power function and SMR for each individual was also estimated and used to obtain $\dot{M}O_2 - SMR$ to correlate with VeDBA.

Fin beat frequency

During trials, fish was recorded by a camera (acA2000-165uc-Basler ace, Basler) at 90 fps with a resolution of 1920 × 1080 pixels above the respirometer. Pectoral fins, tip of snout, and center of body were tracked automatically by using a python package, DeepLabCut (Mathis et al., 2018; Nath et al., 2019). The angle between the center of each pectoral fin and the mid-dorsal line was computed. To understand power distribution of the angle time series over frequency, power spectral density (PSD) was computed for each trial using Welch's averaged periodogram method with a Hann window, averaged over 90 × 10-s segments with 50% overlap. From the PSD, the strongest peak in a frequency range of 1–10 Hz was identified by the scipy.signal.find_peaks function in Python (Jones et al., SciPy: Open Source Scientific Tools for Python, http://www.scipy.org/) and defined as the fin beat frequency.

3D reconstruction of fish posture

Trials were recorded using cameras (acA2000-165uc-Basler ace, Basler) at 90 fps with a resolution of 1920 × 1080 pixels to reconstruct body postures in 3D using Direct Linear Transformation (DLT). Cameras were manipulated using PylonRecorder software (https://gitlab.mpcdf.mpg.de/mpibr/scic/pylonrecorder/PylonRecorder), which enables simultaneous triggering of multiple cameras. Two cameras with 25-mm lenses (25mm C Series Fixed Focal Length Lens, Edmund Optics) were positioned above and on the side of a respirometer.

Using a Python package, DeepLabCut (Mathis et al., 2018; Nath et al., 2019), several marker-less body points of fish were automatically tracked. First, approximately 100 frames were extracted from the videos of each camera and the tip of snout, eye, center of the body, and tail of chromis were manually digitized to create a training dataset. With the dataset, a deep neural network, ResNet-50, was trained to predict the locations of the body points. A readout layer per body point was generated to show the probability of a body point in a particular pixel. Through the training, the readout and deep neural network weights were adjusted. The body points from all the videos were tracked automatically

using the trained model, producing the x-y coordinates in each frame and p-value which shows an accuracy level of the prediction. Tracked points with p-value less than 0.6 and 0.9 for a camera above and on the side of the flume, respectively, were removed and interpolated with a cubic spline interpolation. Lower p-value was chosen for the camera above the flume because occlusion of the body points rarely happened and p-value of >0.6 still produced correct tracking results. Because DeepLabCut treats each frame independently, unrealistic jumps of points in time sometimes occur, which cannot be fully corrected by p-value cutoff. To identify these outliers, the Hampel filter with a window size of 29 and a threshold as a median ±s.d was used. The parameters of the Hampel filter were chosen by confirming that the most of unrealistic jumps were corrected. Detected points were removed and interpolated using a cubic spline interpolation. Finally, data were smoothed with the running mean filter with a window size of five.

To reconstruct body points in 3D from the 2D data of the cameras, the cameras were first calibrated. Camera calibration consisted of intrinsic and extrinsic calibration. Intrinsic calibration concerned camera properties that were independent of the camera position, such as the focal length, image size, and the location of the principal point of each camera. Intrinsic calibration for each camera was performed using the OpenCV package in Python with videos of a checkerboard moving toward the camera. Extrinsic properties involve the position and orientation of the cameras and were estimated with a MATLAB package, easyWand5, which returns DLT coefficients (Theriault et al., 2014). To perform extrinsic calibration, easyWand5 requires videos with a wand swinging over the field of view, a set of pictures of dotted grid paper, a set of pictures of a box with markers specifying the origin and three axes, and the intrinsic properties of each camera. Using DLT coefficients obtained from the extrinsic calibration, two-dimensional coordinates from the videos were transformed into 3D coordinates (Hartley and Zisserman, 2004).

Estimation of Vectorial dynamic body acceleration (VeDBA)

To examine correlation with oxygen consumption rates, vectorial dynamic body acceleration (VeDBA) was obtained from the video. In this study, VeDBA of eye was computed and used for further analysis because marker-less tracking is affected by errors when a body point is not distinguished well. Using the eye position time series in 3D, the second order forward finite difference method was employed to obtain instantaneous acceleration in each axis. VeDBA was calculated as

$$VeDBA = \sqrt{{a_x}^2 + {a_y}^2 + {a_z}^2}, \tag{2.2}$$

where a_x, a_y, a_z are dynamic body acceleration values measured in three orthogonal axes in the earth's frame of reference. Because acceleration measured by an accelerometer includes the gravitational acceleration, DBA and gravitational acceleration are usually separated via moving average smoothing (Halsey et al., 2011). With the video-based method, however, the raw acceleration corresponds to DBA because it does not include the gravitational acceleration. The sampling rate was 90 Hz, the same as the frame rate of the videos. In each trial, mean VeDBA was computed. Despite the data processing applied to the tracked body points, the resulting 3D data still lacked full accuracy. There were two issues encountered. Firstly, a few unrealistic jumps were observed in the 3D data. Secondly, there were several periods where consistently low VeDBA (<0.001 g) was found, corresponding to the periods when the fish was outside the frame. As a solution, VeDBA values >1 g and <0.001 g were excluded when averaging (1 g corresponds to Earth's gravitational acceleration, 9.8067 m s^{-2}). Mean VeDBA and oxygen consumption rates from the two trials for each condition was used to test their relationship. During the oxygen consumption experiments, 3D data for eight out of 60 trials were not measured due

to the malfunctioned camera recordings. In those cases, one of the two trials for each condition was used as a representative.

Oxygen consumption measurements during feeding

The relationship between oxygen consumption rates and VeDBA described above was obtained during steady swimming without foraging behavior. To examine if the relationship can be applied during feeding, measurements of oxygen consumption rates with and without prey injection were conducted at three flow speeds (10, 20, and 30 cm s^{-1}) for three individuals (A–C).

Experiments were conducted following the aforementioned protocol except for differences in flow speeds and prey injection. In detail, each trial comprised a series of six measurement cycles at increasing flow speeds from 10 to 30 cm s^{-1} at increments of 10 cm s^{-1} and two measurements with and without prey injection at each flow speed. Each measurement cycle consisted of 5 min of flush, 2 min of equilibration, and 20 min of measurement. At the second measurement at each flow speed, a total of 1000 prey items were injected gradually over 20 min of the measurement period. Note that the background respiration measurements without fish were conducted both with and without prey injection, but the respiration of the prey had a negligible impact. $\dot{M}O_2$ and VeDBA were then computed as described.

Feeding experiment

Feeding experiments were conducted in a big custom-made flume (Figure 2.3). The flume configuration for experiments on chromis was a modified version of Ishikawa et al.'s (2022). Briefly, the flume was a horizontal recirculating open channel with a rectangular cross section. The test section was 150 cm long and 30 cm wide, filled with water 23 cm deep (changed from 30 cm in Ishikawa et al., 2022). At the inlet and outlet of the test section were flow straighteners and a contraction (diffuser) with a slope of 0.1. Because water sped up in the test section with the contraction, flow speed value on the controller was adjusted to produce the desired flow speed. Water temperature was maintained at 25±0.5°C. Two lights (Mitras lightbar 60, GHL, Germany) were placed above the center of the experimental section and turned on between 07:00 h and 19:00 h (12 h:12 h light:dark).

To examine effects of flow speed, flow speed was controlled to be six levels (5, 10, 15, 20, 25, and 30 cm s^{-1}) to match with the respirometry experiment and under a fixed prey density (1000 m^{-3}). Two replicates were carried out for each flow speed to acquire feeding rates and DBA during feeding.

The feeding experiments were conducted following Ishikawa et al (2022) with some modifications. In summary, one water cycle in this experiment was defined as, based on the average flow speed, the time it took for water to circulate once through the recirculating flume. The designated flow speed was set for ≥30 min prior to the start of a trial and a custom-made 100 μm plankton net with a square frame, tightly fitting the flume's cross section, was used to remove particles from the water in the flume during ≥2 cycles. The water temperature control was turned off and valves were closed to stop the inflow and outflow of fresh seawater, so that seawater simply recirculated in the flume. Through the experiments, water temperature was maintained at 25±0.5°C by the air conditioner in a room. Given the volume of the entire flume, individual live prey were manually counted to obtain the target prey density in each trial. Prey were gradually released downstream of the center section during one water cycle to achieve a nearly homogeneous prey distribution. After the fish started feeding, a trial was started that lasted one water cycle.

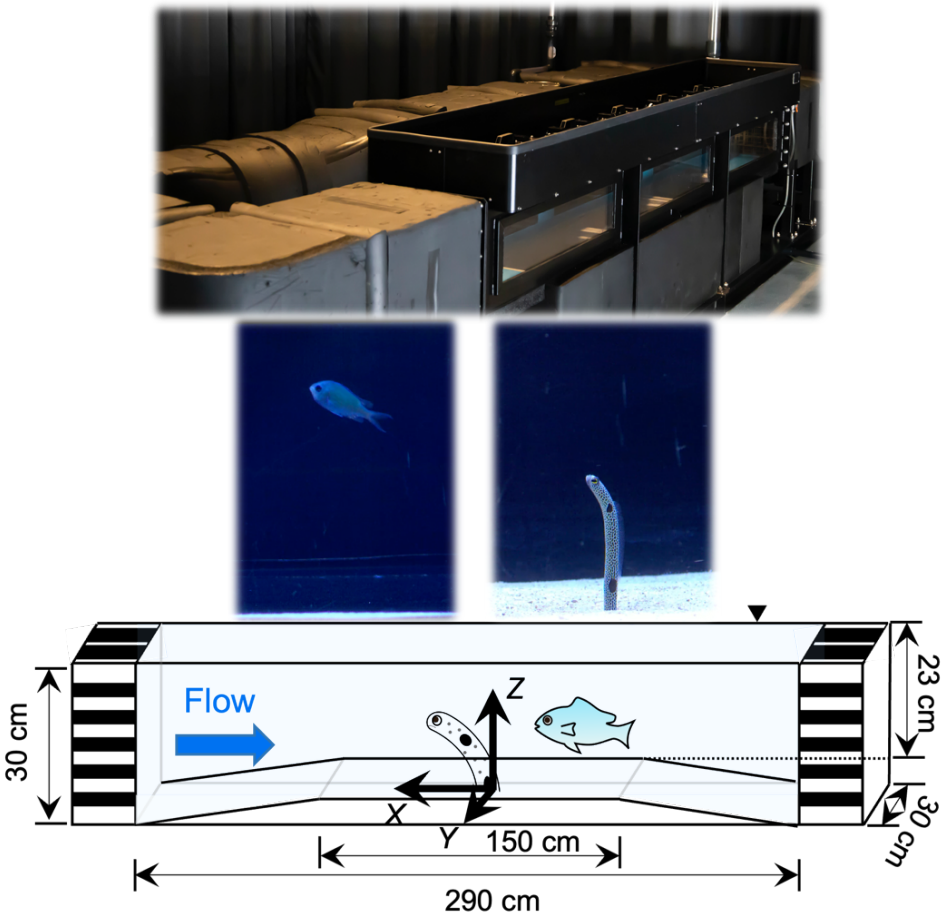

Figure 2.3. Big flume for feeding experiment, images of fish during experiments, and schematic diagram of the test section.

During a trial, the behavior of fish was video-recorded using a camera (EOS R6 Mark II, Canon) at 50 fps with 4K resolution. In the videos, the number of successful strikes, defined as open-mouthed lunges in which prey items entered fish mouths, was counted. To estimate the feeding rate (min^{-1}), number of successful strikes were divided by the time required for one water cycle. Sometimes, fish missed their prey, defined as failed open-mouthed lunges, or gave up pursuing prey, which was defined as a clear movement toward prey, but without a lunge. During the entire series of experiments, only on ≤5 occasions, did fish miss or give up. Thus, the success rate was nearly 100% under all conditions tested.

Energy cost and energy gain

With the measured oxygen consumption rates and feeding rates of chromis at different flow speed, net energy gain was computed as follows.

From the oxygen consumption rate, $\dot{M}O_2$, energy cost per hour (J h^{-1}) at a given flow speed was estimated as

$$E_{cost} = 13.56 \times \dot{M}O_2 \times M, \quad (2.3)$$

where M was the mass of fish (kg), and a conversion rate of 1 mg of O_2 = 13.56 J was applied (Elliott and Davison, 1975). During steady swimming, E_{cost} was computed using measured $\dot{M}O_2$, whereas during feeding, E_{cost} was computed using $\dot{M}O_2$ estimated from the measured VeDBA.

On the other hand, energy gain per hour at a given flow speed was estimated from the feeding rate. The energy gain per hour (J h^{-1}) was computed as

$$E_{gain} = F \times J \times E_{prey}, \quad (2.4)$$

where F is the feeding rate (h^{-1}), J is a constant describing the efficiency of energy yield from prey, accounting for digestion and excretion of fish, which is 0.68 (Hill and Grossman, 1993). E_{prey} is energy content (J) of a copepod which is a major food source of *C.viridis* (Hiatt and Strasburg, 1960). Individual copepod with a body length of 1.0 mm weighs ~16.2 µg (Noda et al., 1992; Pearre Jr., 1980). Based on their energy value per dry weight (11.39 J mg^{-1}DW; Chen et al., 2019), E_{prey} was 0.18 J.

Assuming 12 h of feeding and 12 h of swimming without foraging, net energy gain, E_{net}, was estimated by subtracting E_{cost} of 12 h of foraging and of 12 h of steady swimming from 12 h of E_{gain}. As a function of flow speed, E_{net} was estimated using the power function of $\dot{M}O_2$ during steady swimming and the Lagrange polynomial of $\dot{M}O_2$ and F during feeding. By computing the zero-crossing flow speed of the first derivative of E_{net}, the flow speed at which fish maximize E_{net} was estimated in the range of flow speeds tested (5–30 cm s^{-1}). The maximum E_{net} was set to 1 to compute the relative net energy gain. An arbitrary threshold of 0.9 was used to identify a range of flow speeds at which fish are able to acquire energy efficiently (Hill and Grossman, 1993).

Statistical analysis

To test the relationship between oxygen consumption rates and VeDBA, a generalized linear mixed model (GLMM) fit with REML (Restricted Maximum Likelihood), which treats random effects of dependent data (Bates et al., 2015) was used because the same set of individuals were repeatedly experimented in different flow speed treatments. Data were analyzed by specifying VeDBA as a fixed effect and individuals as a random intercept effect using the lme4 package (Bates et al., 2015) in R (R Core Team 2020). Significance was computed with the lmerTest package (Kuznetsova et al., 2017), which performs analysis of variance to acquire p values by applying the Kenward-Roger's degree of freedom method for mixed models. Marginal and conditional R^2 values were further computed. To test if the inclusion of individuals as a random intercept effect produces a better model, likelihood ratio test was conducted between models with and without the random effect. Because VeDBA is an activity-based proxy, relationship between oxygen consumption rates minus standard metabolic rates and VeDBA was tested in the same way. Also, relationship between fin beat frequency and VeDBA was tested.

2.3. Results

Flow speed in habitats

The field observations revealed that chromis experienced flow speeds up to ~40 cm s^{-1} (Figure 2.4). In the chromis habitat, the mean flow speed was 13.9 cm s^{-1}. Observed chromis spent 33.3% of their time at a flow speed of 5–10 cm s^{-1}, 21.8% at 10–15 cm s^{-1}, and 15.6% at 15–20 cm s^{-1} (Figure 2.4). In the habitat of garden eels, the mean flow speed was relatively slower, with a maximum of ~30 cm s^{-1} and a mean of 8.5 cm s^{-1}. Observed garden eels spent >70% of their time at a flow speed of <10 cm s^{-1}, 19.8% at 10–15 cm s^{-1}, and 5.1% at 15–20 cm s^{-1} (Figure 2.4).

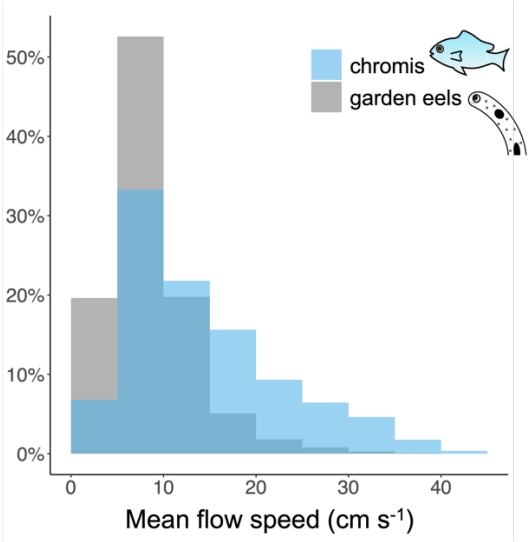

Figure 2.4. Frequency distribution of mean flow speeds in habitats of chromis and garden eels.

Oxygen consumption rates and VeDBA of chromis during steady swimming

In the respirometer, chromis increased their oxygen consumption rates as flow speed increased (Figure 2.5A). The fit of the observed data points from all individuals to the power function describes the relationship between flow speed and oxygen consumption rates as $\dot{M}O_2 = 152.15 + 0.47 \times U^{1.76}$. From the equation, the mean standard metabolic rate (SMR) was estimated as 152.15 mg O_2 kg^{-1} h^{-1}.

Video-based VeDBA of chromis was examined for correlation with oxygen consumption rates under different flow speeds in a respirometer. Oxygen consumption rates and DBA both increased as flow speed increased. Based on the GLMM, there was a significant relationship between oxygen consumption rates and VeDBA (Figure 2.5B; $p<1\times10^{-6}$). Marginal R^2 (only fixed term) was 0.54, and conditional R^2 (fixed term + random term) was 0.78, suggesting that video-based VeDBA is a good proxy of oxygen consumption rates. The likelihood ratio test showed that the model significantly improved by adding individuals as a random factor, suggesting that the model's intercept significantly depends on individuals. When individual difference is considered, VeDBA becomes a better proxy.

VeDBA estimates activity-related energy cost; thus, estimation power decreases as the proportion of non-activity cost increases. In respirometry studies for fish, when oxygen consumption rate is plotted against flow speed and fitted with power function, the oxygen consumption rate at zero flow speed is considered as standard metabolic rate (SMR) which is the minimal amount of energy required for maintenance or resting metabolic rate (Binning et al., 2014; Roche et al., 2013; Schakmann and Korsmeyer, 2023). Therefore, I examined the SMR by fitting the power function for each individual and computed oxygen consumption rates minus SMR to examine the correlation with VeDBA. By GLMM, there was a significant relationship between oxygen consumption rate minus SMR and VeDBA (Figure 2.5C; $p<1\times10^{-6}$). Marginal R^2 (only fixed term) was 0.62, and conditional R^2 (fixed term + random term) was 0.78, suggesting that VeDBA better estimates activity-related energy cost.

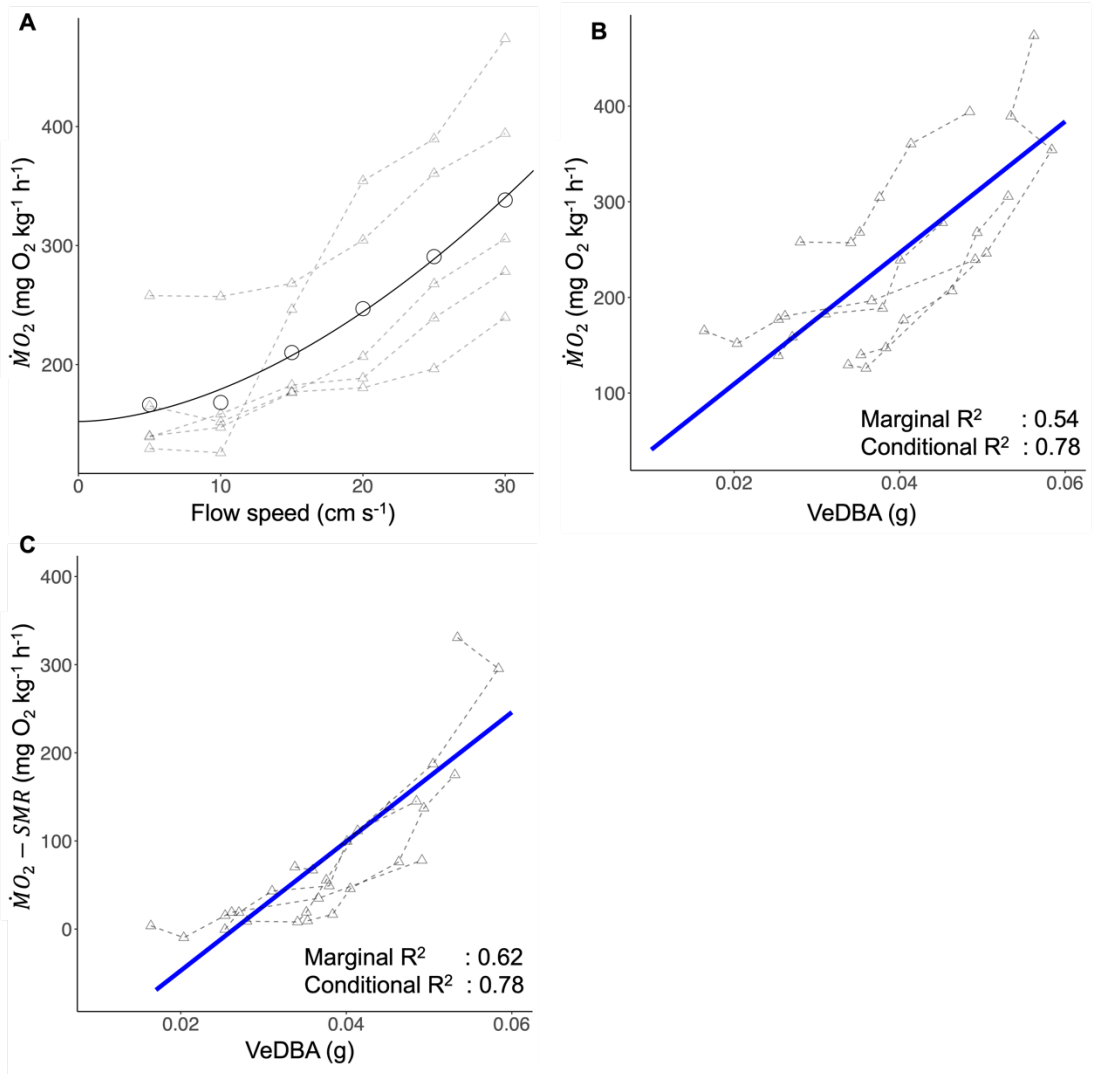

Figure 2.5. Relationship between (A) oxygen consumption rate and flow speed, (B) oxygen consumption rate and VeDBA, (C) oxygen consumption rate minus standard metabolic rate and VeDBA. Triangles and dashed lines in grey indicate relationships in each individual. Solid lines were fitted with (A) power function ($y=a+bx^c$, $p<0.001$), (B,C) GLMM with VeDBA as a fixed effect and individuals as a random intercept effect ($p<1\times10^{-6}$). (A) Circles are means among individuals (n=5).

Oxygen consumption rates and VeDBA of chromis during feeding

When prey was injected in the respirometer, chromis showed feeding behavior which enhanced oxygen consumption rates and VeDBA compared to steady swimming without feeding (Figure 2.6). The linear mixed model based on the data points during steady swimming showed a significant relationship between VeDBA and oxygen consumption rates (Figure 2.6; $p<0.01$). The data points during feeding were mostly within the 95% confidence intervals of the model (Figure 2.6), suggesting that the model from steady swimming can be applied to active feeding behaviors which involves more rapid changes in speed and direction.

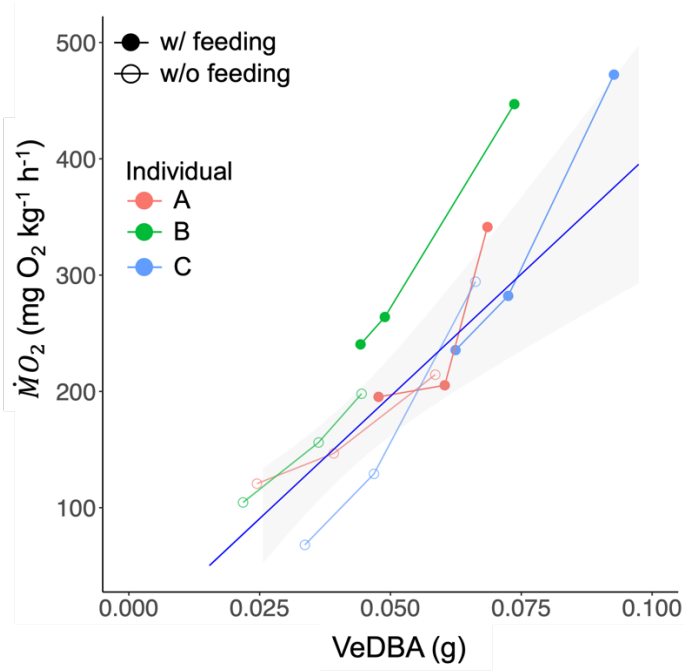

Figure 2.6. Relationship between oxygen consumption rate and VeDBA during non-feeding and feeding. Open circles and filled circles indicate relationships without feeding (steady swimming) and with feeding, respectively. Data points during steady swimming were fitted with GLMM with VeDBA as a fixed effect and individuals as a random intercept effect (p<0.01), and the model was showed as a solid blue line with grey shade indicating 95% confidence intervals.

Fin beat frequency during steady swimming

The power spectral density of angles of a pectoral fin showed a clear peak interpreted as fin beat frequency (Figure 2.7A). Fin beat frequency increased monotonically with flow speed. The relationship between pectoral fin beat frequency (FBF) and oxygen consumption rate ($\dot{M}O_2$) was significant with GLMM (Figure 2.7B; $p<1\times10^{-8}$). Marginal R^2 (only fixed term) was 0.68, and conditional R^2 (fixed term + random term) was 0.86.

Energy cost during feeding

During feeding, VeDBA of chromis increased as flow speed increased (Figure 2.8A). On the other hand, garden eels did not change VeDBA significantly with changes in flow speed (Figure 2.8B). For chromis, VeDBA was converted into oxygen consumption rates using the model obtained in the respirometry experiment. To achieve highest possible accuracy, individual difference was taken into account, and the linear mixed model on oxygen consumption rates minus SMR and VeDBA with individuals as a random intercept effect was used. SMR of each individual was then added back to obtain oxygen consumption rates during feeding (Figure 2.8C).

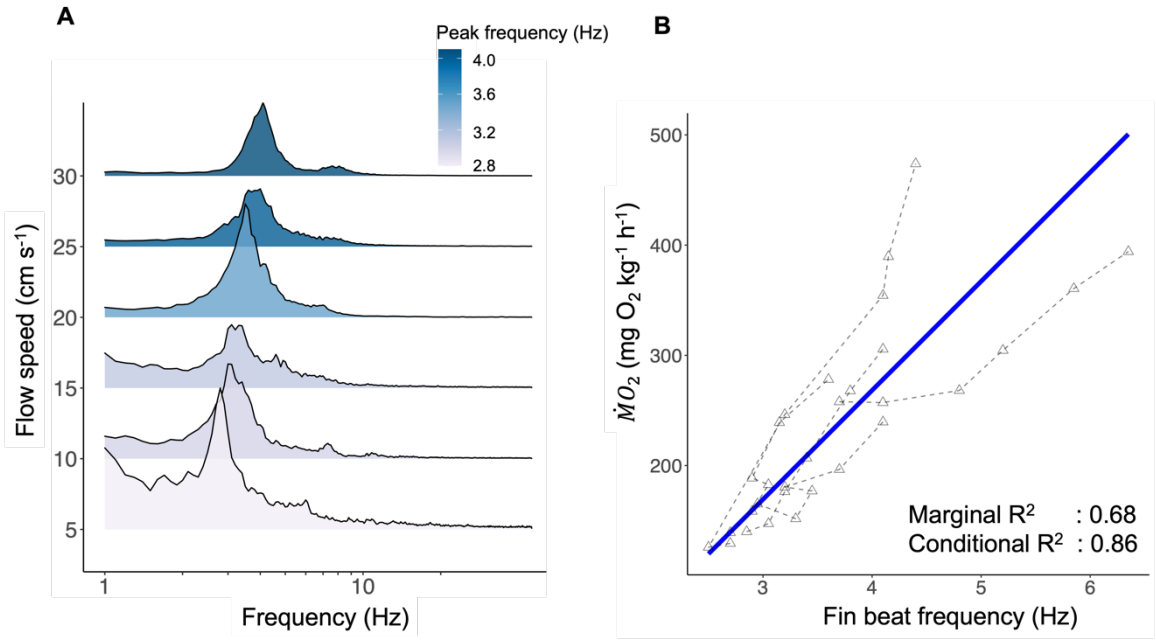

Figure 2.7. The fin beat frequency increased monotonically with flow speed and had a significant relationship with oxygen consumption rates. (A) Power spectral density of angles of pectoral fins for a representative individual was computed at each flow speed. The peaks show fin beat frequency. (B) Triangles and dashed lines in grey show relationships in each individual. The solid line was fitted with the GLMM (p<1×10^{-8}).

Feeding rates

Chromis increased feeding rates up to a flow speed of 25 cm s^{-1} and decreased at 30 cm s^{-1} (Figure 2.9A). On the other hand, feeding rates of garden eels did not significantly change until 20 cm s^{-1} and decreased at 25 cm s^{-1} (Figure 2.9B; Ishikawa et al., 2022).

Cost and benefit model

From oxygen consumption rates during steady swimming in the respirometer, oxygen consumption rates derived from VeDBA during feeding, and feeding rates, I calculated net energy gain of chromis, assuming energy cost from 12 h of feeding and 12 h of swimming and energy gain from 12 h of feeding. Since a prey density of 1000 m^{-3} is the upper end of densities observed in the field (Holzman et al., 2005; Khrizman et al., 2018; Kingsford and MacDiarmid, 1988), cost-benefit models at prey densities of 500, 250 and 100 m^{-3} were further estimated, assuming that feeding rate is a linear function of prey density (Ishikawa et al., 2022; Kiflawi and Genin, 1997). The cost-benefit models showed that chromis can gain excess energy at prey densities >250 m^{-3}, but costs surpass gains regardless of the flow speed when prey density is 100 m^{-3} (Figure 2.10A). The peak of the model, which is the flow speed fish can acquire maximum net energy gain, was approximately at 25 cm s^{-1} at prey densities >250 m^{-3}. Relative net energy gain at a prey density of 1000 m^{-3} was also computed by setting the maximum net energy gain as 1. With the threshold of 0.9, the energetically efficient range of flow speed of chromis was at 16.5–29.3 cm s^{-1} (Figure 2.10B).

For garden eels, although oxygen consumption rate was not quantified, VeDBA during feeding was not significantly affected by flow speeds (Figure 2.8B), suggesting that garden eels can keep a similar level of energy cost regardless of flow speeds. Thus, the shape of net energy gain is expected to be similar to energy gain (feeding rates). To obtain relative

net energy gain of garden eels, I conducted second order polynomial regression on the relationship between flow speed and feeding rates and scaled it by setting the maximum feeding rate as 1. Using an arbitrary threshold of 0.9, the range of flow speed that eels can effectively acquire energy was 7.1–19.3 cm s^{-1} (Figure 2.10B).

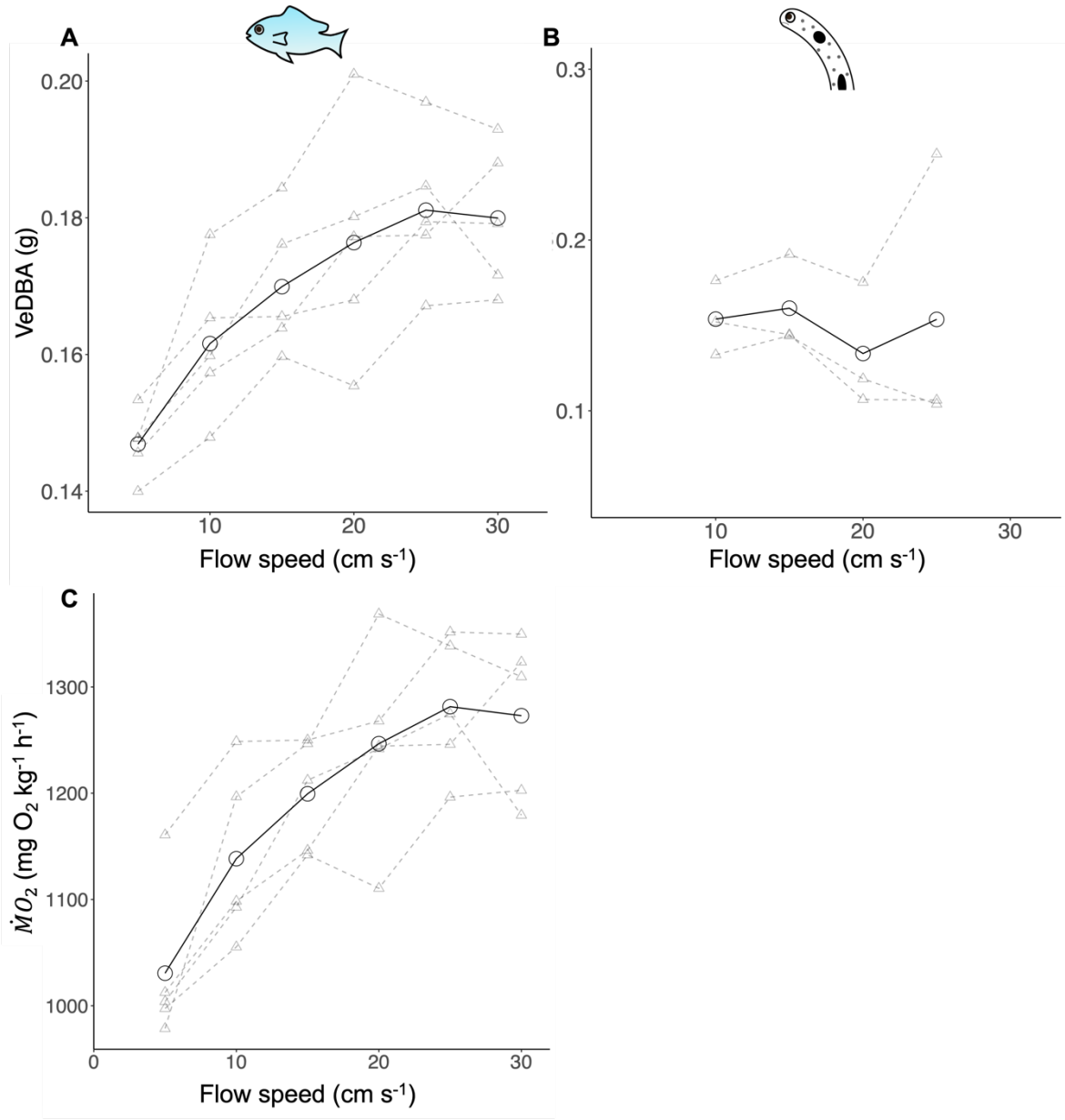

Figure 2.8. Relationship between flow speed and VeDBA and VeDBA-derived oxygen consumption rates. (A) Chromis increased VeDBA as flow speed increased whereas (B) garden eels showed no significant change in VeDBA during feeding. (C) Oxygen consumption rate during feeding was estimated by VeDBA and increased with flow speed. Circles are means among individuals (n=5 for chromis and n=3 for garden eels). Triangles and dashed lines in grey show relationships in each individual. Data for garden eels is from Ishikawa et al. (2022).

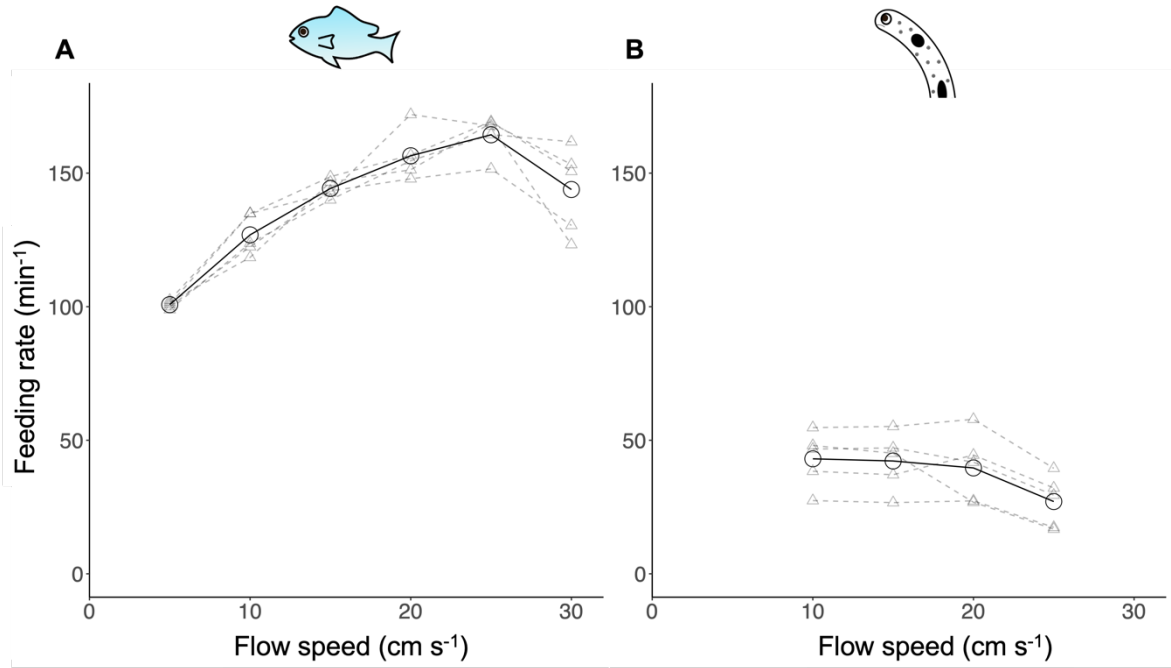

Figure 2.9. Relationships between feeding rate and flow speed. (A) Chromis increased feeding rates at flow speed up to 25 cm s^{-1} and decreased at 30 cm s^{-1}. (B) Feeding rates of garden eels did not decrease until 20 cm s^{-1} but decreased at 25 cm s^{-1}. Circles are means among individuals (n=5) at a fixed prey density of 1000 m^{-3}. Triangles and dashed lines in grey show relationships in each individual.

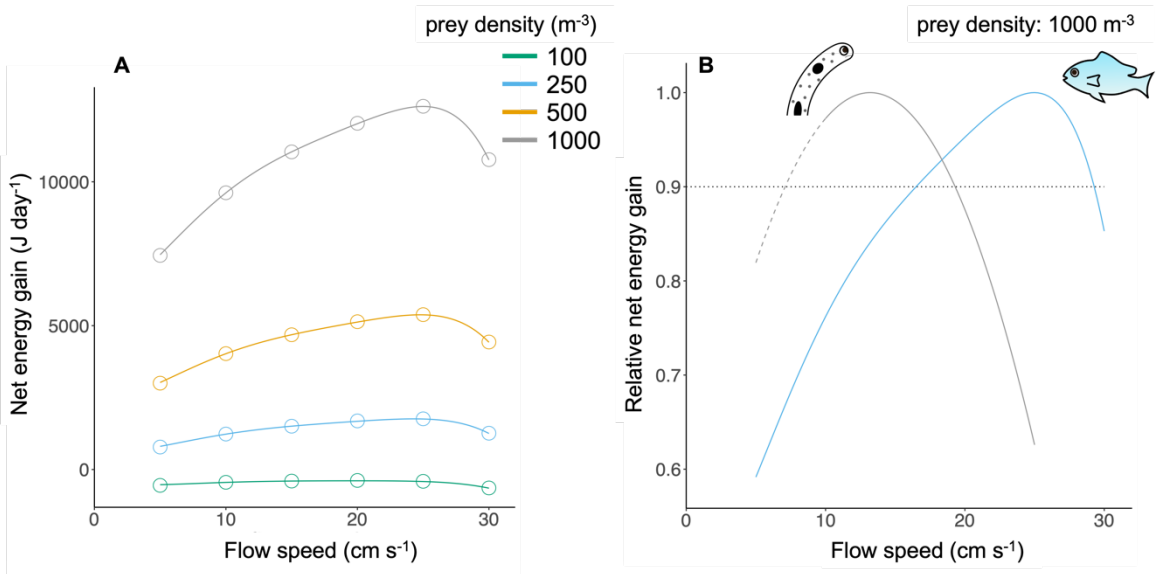

Figure 2.10. Cost-benefit models of chromis and garden eels. (A) The solid line shows the absolute net energy gain of chromis at different prey densities. Data points are means among individuals (n=5). (B) Solid lines show relative net energy gain of chromis in blue and garden eels in grey. Relative net energy gain of eels was estimated from feeding rates, assuming constant energy cost under a range of flow speeds. Dashed line is the range extrapolated. An arbitrary threshold of 0.9 was chosen to indicate a range of flow speed at which fish can efficiently acquire energy.

2.4. Discussions

DBA as a proxy of oxygen consumption rate for small fish

DBA has been shown to highly correlate with oxygen consumption of a wide range of animal taxa (Halsey et al., 2009; Halsey et al., 2011; Lyons et al., 2013; Payne et al., 2011; Robson et al., 2012; Wilson et al., 2020) and used to find new insights in ecology and animal behavior (Grémillet et al., 2018; Rotics et al., 2016; Williams et al., 2014). The most significant limitation of this method results from the attachment of the logger; effects of a logger are a concern, especially for small animals with less than a few hundred grams of body weight. Among vertebrates, species lighter than 100 g occupy 51.5% of mammals, 68.6% of birds, 77.7% of reptiles, 94.6% of amphibians, and 52.7% of fish (O'Gorman and Hone, 2012), and thus should not be overlooked. Even if loggers are seemingly small compared to animals body size, there might be potential effects, especially increased drag during flying or swimming (Pennycuick et al., 2012; Saraux et al., 2011; Vandenabeele et al., 2015; Watson and Granger, 1998).

DBA derived from the video-based method significantly correlated with oxygen consumption rates of damselfish (Figure 2.5), opening applications to all animals. Theoretically, dynamic body acceleration measured by an accelerometer and image processing are the same, leading me to develop the proposed video-based method. Because of the marker-less feature of this method, animals are completely free from any burden, such as implantation or external tag attachment, although marker attachments or dye injection may improve tracking accuracy. An accelerometer records gravitational acceleration during measurement, and thus, gravitational acceleration, which is estimated by taking a running mean, should be subtracted from raw acceleration data to acquire dynamic body acceleration (Shepard et al., 2008). Some cases include fast maneuvers where computed gravitational acceleration is not equal to 1 because of the increased inertial acceleration (Wilson et al., 2013). As gravitational acceleration is not detected with the video-based method, video-based DBA is always only from animal movement. Errors of DBA measured by a logger are also caused by the calibration, position, and stabilization level of the logger (Garde et al., 2022), which are expected to be not crucial in the video-based method.

The video-based method has some limitations derived from its methodology. While the error range is usually consistent in an accelerometer, the error of the video-based method is case-specific caused by the configuration of cameras, tracking, 3D reconstruction. Especially, size of the tracked body points in frames should not be too different between calibration and application. Resolution, light condition, and camera settings may also affect tracking errors. Because DeepLabCut is used for automatic tracking, the accuracy of the model also affects the results. Furthermore, calibration of the 3D reconstruction should be conducted properly to minimize errors. To minimize errors related to these, I suggest that the condition that investigators attempt to apply the calibration curves should be as similar as possible to that where the calibration is made. However, system-dependent error range becomes an advantage when the method is applied to microscale animals because users can determine the size of the subject in an image (e.g., even with a microscope) and enable fine measurement of acceleration.

This method can be applied in fields when animals are likely to stay in the field of view most of the time. For instance, the subject species, *C.viridis*, lives around a coral colony, using the colony as a shelter. If arranged appropriately, the cameras can capture their behavior the whole time, and the acceleration of different behaviors can be measured. However, animals in the field often move large distances or hide in shelters, making it challenging to capture with cameras. In those cases, an accelerometer is a better way to

estimate field metabolic costs. The video-based method is robust in laboratory experiments where users can control these unwanted situations. Also, as suggested by results in this study (significant effects of individual differences), calibration for each individual should be used in an application to achieve the highest possible accuracy, which can be relatively easily done in laboratory experiments. Although respirometry in a flume or chamber has been a standard method to estimate energy cost, the method is largely limited by the small size of chambers to detect small changes in oxygen concentration. For instance, individual energy cost during fish schooling behavior has been an interesting subject of behavioral ecology research but has not been measured by respirometry because of a conflict between the small water volume in a respirometer and the large working volume to minimize wall effects on fish school (Johansen et al., 2010; Noda et al., 2016). Fin beat frequency was used as a proxy of energy expenditure (Johansen et al., 2010; Tudorache et al., 2009). However, such proxies during steady swimming in a respirometer may underrepresent the behaviors in larger volumes which involve rapid changes in speed and trajectory (Gleiss et al., 2010; Marcoux and Korsmeyer, 2019; Tang et al., 2000; Trudel and Boisclair, 1996). During steady swimming, the pectoral fin beat frequency of chromis showed a high correlation with oxygen consumption rates (Figure 2.7). During foraging, nevertheless, fin beat frequency varied extensively, and a clear peak in PSD was not observed, suggesting the weakness of fin beat frequency as a proxy. With the video-based DBA method, as long as each individual can be tracked, energy cost can be estimated by measuring DBA of each individual in a school. Video-based DBA is also advantageous when studying animals engaged in behaviors that necessitate a larger spatial volume, such as feeding. Feeding is expected to require much more energy than steady swimming as it involves rapid acceleration and deceleration by turning and striking. Thus, when investigating energy cost and benefit of feeding behavior, energy consumption should be examined during feeding, not during steady swimming. Here, I measured VeDBA and estimated oxygen consumption rates during feeding using the calibration curves obtained in a respirometer. The oxygen consumption rate derived by VeDBA indicated that during feeding, chromis consumes more oxygen as flow speed increased, and the consumption rate was 3.8–6.8 times more than steady swimming (Figure 2.8). This quantitative measurement during feeding helps to improve the cost-benefit model discussed below. Because extrapolation of the calibration curve was necessary to estimate oxygen consumption rates during feeding, estimated oxygen consumption rate is expected to include some errors. However, at least in the respirometer, I showed that $\dot{M}O_2$–VeDBA relationship obtained during steady swimming is useful during feeding (Figure 2.6), suggesting that this method likely provides an accurate estimation of energy cost during feeding among methods currently available for small fish.

Although validation with another method is warranted, the video-based DBA is also useful for the relative estimation of energy cost of species for which respirometry is practically challenging, considering DBA's effectiveness in the wide variety of animal species. By measuring DBA of the big black spot on garden eels, their energy costs were relatively compared in a range of flow speeds. The lack of significant changes in DBA (Figure 2.8B) probably resulted from the energy savings by reduced exposure of the body outside the burrow and reduced drag of the bended body at faster flow speeds (Ishikawa et al., 2022). Compared to free damselfish, this is a completely different response to flow speed, highlighting their unique strategy to flows.

Feeding rate of chromis and garden eels

Feeding rates of reef fish usually show a dome-shaped curve in response to flow speed, where feeding increases at slow flows, remains constant at moderate flows, and decreases

at faster flows (Clarke et al., 2009; Ishikawa et al., 2022; Kiflawi and Genin, 1997). The feeding rates of chromis in this study agreed with these previous studies (Figure 2.9A). Compared to the flume study on *Dascyllus marginatus* and *Chromis viridis* by Kiflawi and Genin (1997), in which the maximum feeding rate occurred at <15 cm s^{-1}, feeding rates of *C. viridis* in this study increased up to 25 cm s^{-1}. Beside interspecific differences, this difference may be associated with flow speed in natural habitats. Mean and maximum flow speeds observed in reefs around habitats of *D. marginatus* and *C. viridis* in the Red Sea are ~5 cm s^{-1} and ~20 cm s^{-1}, respectively, which are less than half of those in the habitat of *C. viridis* in Okinawa (Figure 2.4; Reidenbach et al., 2006). Even within the same species living in two different flow regimes around an island, fish show morphological and physiological variations that are suitable for each habitat (Binning et al., 2014), suggesting that long-term exposure to different flows may have caused evolutionary adaptation of the same species to each environment. For river fish, reduction in feeding rate at high flow speed is associated with reduced capture success (Hill and Grossman, 1993; Piccolo et al., 2008). However, chromis captured almost all nauplii they struck in our experiment, suggesting that their maneuverability as a median-paired fin swimmer enables body control even at fast flows.

Feeding rates of chromis are controlled by the reactive volume, a wedge calculated from empirical reactive distance and angle. As flow speed increases, fish narrow the angle to avoid being oriented lateral to the flow, which causes the risk of being swept down-current (Kiflawi and Genin, 1997). Feeding rates are controlled by the balance between the reduced reactive volume and increased prey flux, showing a dome-shaped curve, a peak of which was observed around 25 cm s^{-1} (Figure 2.9A). On the other hand, feeding rates of garden eels are controlled by the balance between prey flux and exposed body length. As flow speed increases, prey flux increases, whereas exposed body length decreases. Because the extent of the two changes is similar at 10–20 cm s^{-1}, a consistent feeding rate was observed (Ishikawa et al., 2022; Figure 2.9B). At 25 cm s^{-1}, the extent of the decrease in exposed body length surpassed that of the increase in prey flux, resulting in a reduction of feeding rate. From the feeding rates, chromis are more adapted to faster flow speed than garden eels. Although the trends correspond with flow speed in their habitat (faster flow speed observed in chromis habitat), it is important to combine energy gain and cost to make cost-benefit models for further discussion, which will be addressed in the next section.

Cost-benefit model

Combining both energy gain through feeding success and energy expenditure through oxygen consumption and DBA measurements as a function of flow speed, I developed cost-benefit models demonstrating that an energy-efficient range of flow speed for chromis is 16.5–29.3 cm s^{-1} at high prey density. This flow speed range for chromis, a pectoral fin swimmer, covers intermediate to high flow speeds observed in coral reefs, corresponding to studies that suggest adaptations of pectoral fin swimmers to rougher flow environments (Finelli et al., 2009; Fulton and Bellwood, 2005; Marcoux and Korsmeyer, 2019; Schakmann and Korsmeyer, 2023). This range of flow speeds comprised about a quarter of chromis activity in the field (Figure 2.4).

Although net energy gain of garden eels was not quantified, its trend with flow speed is expected to be similar to their feeding rates because of the lack of significant changes in energy cost estimated from VeDBA. Because feeding rates and flow speed usually show dome-shaped curve in planktivorous fish (Clarke et al., 2009; Kiflawi and Genin, 1997), the relationship between feeding rate and flow speed was regressed with a second order polynomial, and relative energy gain was computed by scaling with the maximum for

comparison. The model showed that flow speed range that garden eels feed effectively was 7.1–19.3 cm s^{-1}, which dominates a half of time in their habitat (Figure 2.4; Figure 2.10C).

The distinct peaks in the cost-benefit models of chromis and garden eels indicate that the two fish have different energetically preferred flow speed ranges (Figure 2.10C). These flow speed ranges corresponded well with the flow speed observed at each habitat, suggesting that flow speed is one of the important factors for habitat distributions of planktivorous reef fish. Effects of other factors, such as physical environments and predation pressure, are worth examining in future studies to improve our understanding of their habitat selection and adaptation.

Although chromis and garden eels spend a quarter and half of their time in a cost-effective range of flow speed, respectively, they need to spend rest of the time which is suboptimal to maximize net energy intake. This inconsistency may result from limitations of our model. The cost-benefit models may include errors from various sources. For example, although I examined effects of unidirectional flows, oscillatory flows significantly increase oxygen consumption of reef fish (Marcoux and Korsmeyer, 2019; Schakmann and Korsmeyer, 2023). The field measurements indicate that especially the chromis habitat is dominated by wave-induced oscillatory flows, with frequencies of 0.1–0.5 Hz. Also, I used *Artemia* nauplii to eliminate possible effects of changes in prey movements in response to flows. In nature, however, both chromis and garden eels feed on copepods and other marine zooplankton (Donham et al., 2017; Hiatt and Strasburg, 1960) with stronger escape behavior, which may affect foraging performance (Clarke et al., 2005). Moreover, prey size distribution in nature depends on flow speed, such that larger plankton can be found at faster flows (Hill and Grossman, 1993; Jenkins and Keeley, 2010). By accounting for these factors, the models might be improved in future studies.

2.5. Chapter Conclusion

By combining recent advances in automatic tracking techniques and dynamic body acceleration, I developed the video-based method to estimate energy expenditure of animals. The approach enables estimating energy costs without some of the limitations, such as confined small chambers and attachment or implantation of loggers. Using the method, I estimated energy costs of chromis and garden eels during feeding, which was impractical without it and helped to develop more accurate cost-benefit models involving energy cost during feeding. This technique can be applied to any animals but is especially useful for small animals, to which the conventional DBA method with an accelerometer cannot be applied.

By measuring oxygen consumption rates, VeDBA, and feeding rates as a function of flow speed, empirical energy cost-benefit models for site-attached damselfish and anchored garden eels in coral reefs were developed. The derived ranges of flow speeds at which fish efficiently acquire energy showed a good agreement with the flow speeds observed in their natural habitats, suggesting that the flow speed is a key factor for the ecology of zooplanktivorous fish in coral reefs. The models can be applied to estimate habitat distributions and to assess environmental quality, which may guide conservation efforts in the face of coastal development around coral reefs.

Chapter 3

Effects of Small-Scale Turbulence on Planktivory by Anchored Garden Eels and Site-Attached Fish

3.1. Introduction

In Chapter 1 and 2, I demonstrated how mean flow speed affects feeding and metabolism of planktivorous fish in coral reefs. Effects of mean flow speed on fish have been investigated extensively. Using flumes and water tunnels, other research has also shown effects of mean flow speed on fish swimming behavior (Heatwole and Fulton, 2013), feeding behavior (Kiflawi and Genin, 1997; O'Brien et al., 2001; Piccolo et al., 2008), sheltering behavior (Johansen et al., 2008b), and energy consumption for locomotion (Fausch, 1984). These experiments have been conducted with honeycombs to regulate flows and focused on effects of mean flow speed to simplify the hydrodynamic environment. However, the flows produced in these experiments may underrepresent complexities of flows in natural environments.

To advance understanding of the effects of flows, recent studies have examined effects of more complex flows on fish (Higham et al., 2015; Liao, 2007; Trinci et al., 2017). One of the ways to add complexities in a laboratory flume is to place structures such as cylinders. Fish alter their behavior around a cylinder; reduced body movement and swimming at low velocity in front of a cylinder (bow-waking), angling the body into the mean flow direction (entraining), and synchronizing body rhythm with the Karman vortex street behind the cylinder were observed (Karman-gaiting; Liao 2007). Other studies that used cylindrical structures, turbines, and specific wall shapes found complex flows influence fin beating, swimming speed, stabilization, and oxygen consumption (Lupandin, 2005; Maia et al., 2015; Roche et al., 2014). The complex flows generated in these studies, however, often include strong energy in a specific frequency that fish may be able to learn and adapt in a short period. To precisely assess effects of turbulence, it is necessary to generate turbulence with more stochasticity.

To avoid flows being dominated by a specific frequency in flumes, grid-generated turbulence was used to study its effect on oxygen consumption of shiner perch (van der Hoop et al., 2018). The fish decreased oxygen consumption under stronger turbulence, but the mechanism of reduced energy expenditure was unclear. Moreover, previous studies on effects of complex flows mainly focused on fish locomotion or movement. As complex flow is expected to affect both prey movement and fish behavior, its effect on feeding warrants further investigation (Clarke et al., 2009). Furthermore, most studies have focused on fish that swim freely to capture zooplankton, whereas there are few studies on anchored fish, like garden eels, that forage with their bodies anchored to the substrate. These eels rely on flows for their food supply because their movements are constrained by their dependence on semi-permanent burrows (Smith, 1989). As discussed in Chapter 1 and 2, garden eels show unique responses to changes in mean flow speeds, but effects of turbulence are unknown.

When studying effects of turbulence on aquatic animals in the laboratory, the ecological relevance of turbulence levels is often validated by citing other studies that measured turbulence in an environment where the subject species is likely to live. However, turbulence levels in the laboratory may not represent those experienced by aquatic animals (Franks et al., 2022; Peters and Redondo, 1997). Also, in some cases, it is unclear whether the species used in laboratory experiments exists in field sites.

In this chapter, I compared effects of grid-generated turbulence on zooplanktivory by free damselfish and anchored garden eels by combining field flow measurements and controlled flume experiments. Feeding attributes examined included 3D foraging movements and feeding rates. Garden eels and chromis showed differential responses to grid-generated turbulence in a flume, showing fits to the flow environment in each habitat.

3.2. Methods

Flow measurements in the field

Flow measurements were made at habitats of chromis and garden eels as described in Chapter 2 (Figure 2.1) and further analyzed as follows to acquire several turbulence parameters.

Based on the principal axis of water motion, instantaneous velocities at site A were rotated into coordinates such that x was across-shore, y was along-shore, and z was vertical (with upward being positive) while those at site B were rotated into coordinates such that x was along-shore, y was across-shore, and z was vertical. Axes with 350˚ and 250˚ from true north were defined as the positive directions of principal axes for sites A and B, respectively (Figure 3.1). Velocity data were screened for low beam correlations (<60%) and missed data were interpolated. Mean flow speed was computed by averaging flow velocities in the *x*-*y* plane over each 10-min burst.

Instantaneous velocities (u, w) in x and z directions can be decomposed as

$$u = \bar{u} + u' + \tilde{u};\ w = \bar{w} + w' + \tilde{w}, \tag{3.1}$$

where $\bar{u}$ and $\bar{w}$ are temporally averaged velocities, u' and w' are velocity fluctuations due to turbulence, and $\tilde{u}$, $\tilde{w}$ are wave-induced orbital velocities. To separate wave components from turbulence, I applied the Phase method (Bricker and Monismith, 2007) that converts temporal velocities into frequency space using Fourier transformation and isolates wave stress as a clear wave peak. Mean velocity and turbulence statistics were computed by averaging over each 10-min measurement (Gross and Nowell, 1983). For each 10-min measurement, power spectra of w were computed using Welch's averaged periodogram method with a Hann window, averaging over 10 × 1-min segments with 50% overlap. From vertical, one-dimensional power spectra, the range of frequencies with wave peaks and noise floor were identified empirically.

To compute the dissipation rate (ε) of turbulence kinetic energy (TKE), which is the rate at which TKE is dissipated by viscous forces, I used a one-dimensional spectrum of vertical velocity fluctuations, following Hench and Rosman (2013). Assuming that the frozen turbulence hypothesis holds, the power spectral density S as a function of frequency f is written as:

$$S(f) = \frac{24}{55}\alpha\left(\frac{\bar{u}}{2\pi}\right)^{\frac{2}{3}}\varepsilon^{\frac{2}{3}}f^{-\frac{5}{3}}, \tag{3.2}$$

where α=2.0 is the Kolmogorov constant, and $\bar{u}$ is the temporally averaged flow velocity (Pope, 2000). After isolating the wave peak using the Phase method and removing the noise floor, I fit a –5/3 slope to the inertial subrange. Only –5/3 slope lines with an $r^2 \geq 0.25$ were used to acquire the dissipation rate to ensure a well-defined inertial subrange and minimum contamination due to waves.

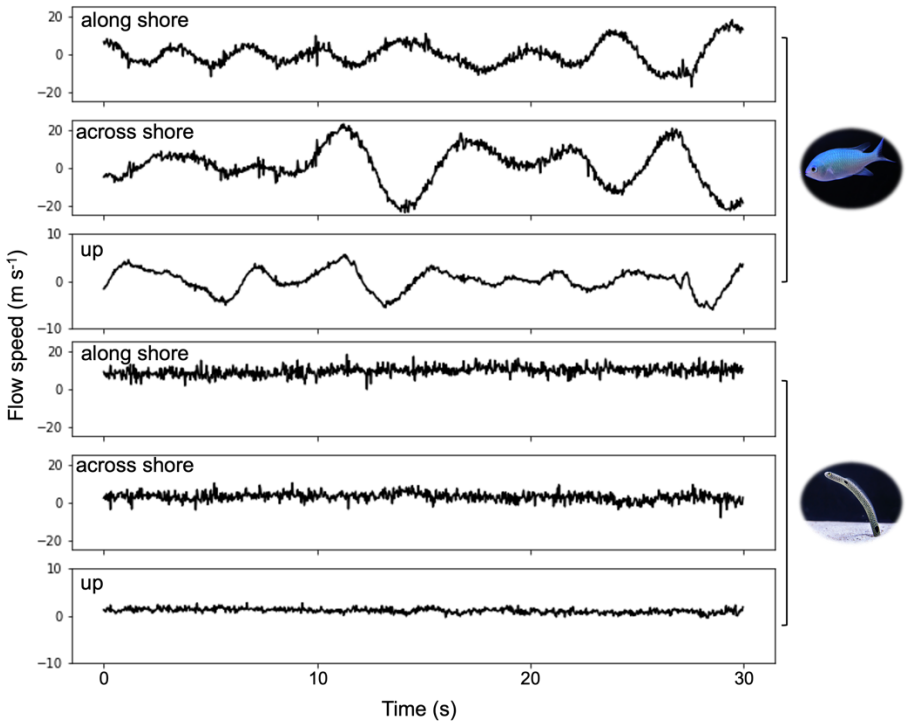

Figure 3.1. Representative recordings by ADV showing flow speeds in the along-shore, across-shore, and upward directions over a 30 s measurement period. The mean flow velocities over the 30 s were approximately 0.1 m s^{-1}.

Reynolds stress, which is the turbulent momentum flux closely related to turbulent mixing, was computed following Bricker and Monismith (2007). Assuming there was no interaction between turbulence and waves, the turbulent Reynolds stress was estimated as

$$\overline{u'w'} = \overline{uw} - \overline{\tilde{u}\tilde{w}}, \quad (3.3)$$

where $\overline{uw}$ is total stress, $\overline{\tilde{u}\tilde{w}}$ is wave stress, and overbar denotes averaging over time. Wave stress was computed through the spectral sum

$$\overline{\tilde{u}\tilde{w}} = \int_{-\omega_{Nyquist}}^{\omega_{Nyquist}} S_{\tilde{u}\tilde{w}}(\omega)d\omega, \quad (3.4)$$

where $S_{\tilde{u}\tilde{w}}$ is the two-sided cross spectral density of wave-induced orbital velocities and ω is frequency (Bricker and Monismith, 2007). Using this method, I computed turbulent Reynolds stress for each 10-min burst. Similarly, components of TKE ($\overline{u'u'}$, $\overline{v'v'}$, and $\overline{w'w'}$) can be computed. Although TKEs calculated by this method tend to have a large error because of the squared terms of each component (Hansen and Reidenbach, 2017), I reported them as a reference (Figure 3.4).

Setup for feeding experiment

The experiments were conducted in a custom-made flume described in Chapter 2 with some modifications (Figure 2.3). Briefly, the flume was a horizontal recirculating open channel with a rectangular cross section. The test section was 150 cm long and 30 cm wide, filled with water 18 cm deep. At the inlet and outlet of the test section were flow straighteners and a contraction (diffuser) with a slope of 0.1. For experiments on garden eels, the bottom center of the test section was replaced with a custom-made sand box to create a sandy bottom in which an eel could make a burrow. The X-axis was defined as the streamwise direction with the upstream direction designated as positive. The Y-axis was defined as the lateral direction. The Z-axis was perpendicular to the bottom with upward

being positive. The origin of the coordinate system was placed at the center of the test section for chromis and at an eel burrow. Water temperature was maintained at 25±0.5°C. Two lights (Mitras lightbar 60, GHL, Germany) were placed above the center of the experimental section and turned on between 07:00 h and 19:00 h (12 h:12 h light:dark).

Two spatiotemporal mean flow speeds, U, of 0.05 and 0.15 m s^{-1} at the center of the test section (averaged over an area of approximately 5 × 5 cm) were used in the experiments. The Reynolds number was defined as UD_h/ν, where ν is kinematic viscosity taken as 9.5×10^{-7} m^2 s^{-1} for seawater with a salinity of 35 ‰ and a temperature of 25 ˚C, and D_h is hydraulic diameter defined as $4A/P$, where A is cross sectional area and P is wetted perimeter. The corresponding Reynolds numbers were 1.7×10^4 and 5.2×10^4 at 0.05 and 0.15 m s^{-1}, respectively and exceeded the often used threshold of 2000–3000 (Avila et al., 2011; Chow, 1959; Schlichting and Gersten, 2017), indicating the flow to be fully turbulent.

To increase turbulence levels, a stationary grid with rods thickness d of 0.5 cm and spacing M of 2 cm was introduced 35 cm or 25 cm upstream from the center of the experimental section. The design of the grid was based on the balance between the resulting turbulence intensity and quality of flow, such as consistent isotropy in the streamwise direction (Lavoie et al., 2007; Olivieri et al., 2021). Given the geometry of the grid, the distance needed for turbulent flow to develop was about 20 cm (Olivieri et al., 2021), which was taken into account when designing the location of the grid. Turbulence without the grid was expected to be the weakest, whereas that with the grid 25 cm upstream from the center was expected to be the strongest at each flow speed.

Flow measurements in the laboratory

For flow visualization and quantification of turbulence parameters in each condition, particle image velocimetry (PIV) was used. PIV yields 2D velocity fields with a laser sheet in a fluid seeded with tracer particles (Raffel et al., 2007). A continuous PIV system was implemented to measure streamwise and vertical velocities, u and w, respectively. The PIV system consisted of an 8W continuous green laser with a wavelength of 532 nm (Omicron-Laserage Laserprodukte GmbH, Germany), a camera (Kato Koken, Japan) to capture 1024 × 1024 pixel images with a field of view approximately 16 cm × 16 cm (±8 cm X direction and 0–16 cm in Z direction). The laser beam emitted from the laser head was reflected by a mirror to orient it downward, perpendicular to the bottom of the test section of the flume and spread into a thin laser sheet with a series of cylindrical lenses (Thorlabs Inc., US). The laser sheet illuminated the seeded particles which were silver-coated, hollow glass spheres with a mean diameter of 10 μm and an average specific gravity of 1.4 (Dantec Dynamics A/S, Denmark). Scattered light was captured by the high-speed camera at 50 and 120 Hz at flow speeds of 0.05 and 0.15 m s^{-1}, respectively. Captured image sequences were processed with a PIVlab tool in MATLAB (Thielicke, 2014; Thielicke and Sonntag, 2021; Thielicke and Stamhuis, 2014) with a recursive grid of 64 × 64 pixels to 32 × 32 pixels and maximum displacement of 0.49. Particles in each grid in an image pair were correlated using an FFT correlator to estimate flow velocity in pixel units. Image units were converted to m s^{-1} with a known time separation between image pairs and a calibration image that was a picture of a ruler. For each trial, 8000 images were acquired to ensure convergence in mean and second order turbulence properties.

In laboratory experiments, instantaneous velocity in the streamwise direction was decomposed into two parts following Reynolds decomposition,

$$u = \bar{u} + u', \tag{3.5}$$

where $\bar{u}$ was the temporal average of the streamwise velocity and u' was the fluctuation. By the same means, velocities in vertical direction w were decomposed into $\bar{w}$ and w'. Power

spectra of w were computed using Welch's averaged periodogram method with a Hann window, averaging over 10 × 800-frame segments with 50% overlap. With the velocity measurement, several spatio-temporally averaged turbulence parameters were computed. Temporal averaging was conducted over 8000 images, and spatial averaging was conducted over a field of approximately 5 × 5 cm at the center of the test section to exclude potential wall effects. As PIV measurements only give 2D velocity fields (u and w), velocity fluctuation in the lateral direction (v') was approximated as a vertical direction (w').

To estimate the dissipation rate of TKE, a method using available velocity gradients from the PIV measurement and least amount of assumptions was applied (Doron et al., 2001). Dissipation rate (ϵ) was defined as

$$\epsilon = 2\nu\langle\overline{S_{ij}S_{ij}}\rangle, \tag{3.6}$$

where $\langle\cdot\rangle$ denotes spatial averaging, the overbar denotes temporal averaging, ν is the kinematic viscosity, and S_{ij} is the strain rate tensor.

Applying the divergence-free continuity equation and assuming local isotropy, Eq. (3.6) was expressed using measured velocities in the X-Z plane

$$\epsilon = 4\nu\left\langle\left(\overline{\frac{\partial u'}{\partial x}}\right)^2 + \left(\overline{\frac{\partial w'}{\partial z}}\right)^2 + \overline{\frac{\partial u'}{\partial x}}\,\overline{\frac{\partial w'}{\partial z}} + \frac{3}{4}\left(\overline{\frac{\partial u'}{\partial z}} + \overline{\frac{\partial w'}{\partial x}}\right)^2\right\rangle \tag{3.7}$$

where $\langle\cdot\rangle$ denotes spatial averaging and the overbar denotes temporal averaging.

TKE was computed as

$$k = \frac{1}{2}\left\langle\overline{u'^2} + 2\overline{w'^2}\right\rangle, \tag{3.8}$$

where $\langle\cdot\rangle$ denotes spatial averaging and the overbar denotes temporal averaging.

Reynolds shear stress was defined as

$$\tau = -\langle\overline{u'w'}\rangle, \tag{3.9}$$

where $\langle\cdot\rangle$ denotes spatial averaging and the overbar denotes temporal averaging.

Fish studied

Chromis and garden eels were purchased from Aqua Planning Co., Ltd. Both species are distributed widely in the Indo-Pacific Ocean and are common in Okinawa. Five garden eels, designated A to E, with total lengths of 29.7, 26.0, 25.8, 26.2, and 26.5 cm, and five blue-green chromis, designated A to E, with body lengths of 3.8, 3.7, 3.7, 3.9, and 3.7 cm, respectively, were used in our experiments. Day-old brine shrimp (*Artemia salina*) nauplii, 0.59±0.05 mm (mean±SD, n=60) in length were used as prey. Different combinations of turbulence levels and flow speeds were randomly assigned and up to five trials were carried out each working day between 9:00 h and 17:00 h (ZT2–ZT10). During ≥3 days of acclimation prior to the onset of trials, designated fish were fed *ad libitum* at a flow speed of 0.05 m s^{-1}. All experiments were conducted with approval from the Animal Care and Use Committee at Okinawa Institute of Science and Technology Graduate University.

Feeding experiments

To examine effects of turbulence, three turbulence levels (without the grid, with the grid at 35 cm upstream, and with the grid at 25 cm upstream) were used at each of the two flow speeds (0.05 and 0.15 m s^{-1}). At each condition, feeding experiments were conducted in the same way as chapter 2. Two replicates were carried out for each condition to acquire feeding rates and foraging movements.

Feeding rate and success rate

During a trial, I video-recorded the behavior of fish using a camera (acA2000-165uc-Basler ace, Basler) at 95 fps with a resolution of 1920 × 1080 pixels. In the videos, we counted the number of successful strikes, defined as open-mouthed lunges in which we saw prey items enter fish mouths. To estimate the feeding rate (number of nauplii min^{-1}), the number of successful strikes was divided by the time required for one water cycle. Sometimes, fish missed their prey, defined as failed open-mouthed lunges, or gave up pursuing prey, which was defined as a clear movement toward prey, but without a lunge. The number of those cases was counted and added to the number of successful strikes to yield the number of pursuits which was used to divide the number of successful strikes to finally yield the success rate. For chromis, the success rate was not calculated because during the entire series of experiments, only on 5 occasions, did fish miss or give up. The success rate was nearly 100% under all conditions tested.

3D reconstruction of fish posture

Experiments were recorded using cameras (acA2000-165uc-Basler ace, Basler) at 95 fps with a resolution of 1920 × 1080 pixels to reconstruct body postures in 3D using Direct Linear Transformation (DLT). Cameras were manipulated using PylonRecorder software (https://gitlab.mpcdf.mpg.de/mpibr/scic/pylonrecorder/PylonRecorder), which enables simultaneous triggering of multiple cameras. For experiments on chromis, two cameras with 25-mm lenses (25mm C Series Fixed Focal Length Lens, Edmund Optics) were positioned above the flume and a camera with a 100-mm lens (C-Mount 12.5-75mm Varifocal Lens, computar) was positioned on the side. For experiments on eels, two cameras with 25-mm lenses (25mm C Series Fixed Focal Length Lens, Edmund Optics) were positioned on the side. Recordings covered the full duration of each trial.

Label-free automatic tracking and 3D reconstruction of fish behavior was conducted following Ishikawa et al. (2022) and chapter 2. In short, the python package, DeepLabCut (Mathis et al., 2018; Nath et al., 2019) was used to digitize body parts of each fish, the mouth, the eye, and the center of the body for chromis and the eye and the first large black spot closest to the eye for eels. Digitized points were filtered with the median filter using a window size of 9. 2D coordinates of body features were then transformed into 3D coordinates with DLT coefficients, using MATLAB package, easyWand5 (Hartley and Zisserman, 2004; Hedrick, 2008; Theriault et al., 2014).

Analysis of foraging movements

For each successful strike, the time and location of its initiation were defined as the point at which a fish started to move toward the prey. Initiation of a strike was clearly visible in video records. As described in Ishikawa et al. (2022), the following four foraging parameters were defined and computed from the 3D coordinates of the fish. Strike time: the duration (s) between strike initiation and prey capture. Strike distance: the distance (cm) between the head of the fish at strike initiation and at prey capture. Strike speed: strike distance divided by strike time ($cm\ s^{-1}$). Reactive distance: the distance (cm) between the head of the fish and the prey at the instant of strike initiation. Ten strikes for each trial were used to estimate the above parameters for each of the aforementioned combinations of turbulence level and flow speed. For eels, the length of the body outside the burrow, defined as the distance r of the digitized positions of the eye, was also measured and compared under different flow conditions. Furthermore, to estimate relative energy consumption, VeDBA was computed following the method described in Chapter 2.

To understand space use by fish, I conducted 2D kernel density estimation on all positional data of the center of the body for chromis and the eye for eels in X-Z and X-Y

planes. Using the kde2d function in the MASS package in R (R Core Team 2020), I calculated the 2D kernel density for 50 × 50 grids, sorted the density values in ascending order, integrated the densities, and picked the grids that reached 0.8 to estimate areas that fish use with 80% probability. Estimated 80% space use was compared among different flow conditions.

Statistical analysis

Statistical analysis was conducted by a linear mixed model fit with REML (Restricted Maximum Likelihood), which treats the random effects of dependent data. Data were analyzed specifying turbulence level as a fixed effect and individuals as a random intercept effect at each flow speed using the lme4 package (Bates et al., 2015) in R (R Core Team 2020). Significance was computed with the lmerTest package (Kuznetsova et al., 2017), which performs analysis of variance to acquire *p* values by applying Kenward-Roger's degree of freedom method for mixed models. Similarly, significance for multiple comparisons was computed with the lsmeans package (Lenth, 2016), which obtains least-square means and computes *p* values adjusted with the Tukey post-hoc test, using Kenward-Roger's degree of freedom method for contrasts. *p* values lower than 0.05 are indicated as * on graphs. In detail, at each flow speed, effects of turbulence levels on feeding rates, success rate, foraging parameters, VeDBA, length, and area use were modeled with the turbulence level as a fixed effect and individuals as a random effect.

3.3. Results

Flow conditions in natural habitats and in the laboratory

The in situ current measurements indicated that the two species experienced different flow speeds and turbulence levels (Figure 3.2B,D). Here, I focused on dissipation rates because turbulence is controlled by local energy dissipation at plankton-length (millimeter) scale involved in the feeding of zooplanktivorous fish (Jiménez, 1997). In chromis habitat, mean flow speeds of <0.1, 0.1–0.2, and >0.2 m s^{-1} existed 40.1, 37.4, and 22.5% of the time, respectively. In garden eel habitat, they comprised 72.2%, 24.8%, and 2.9%, respectively. Dissipation rates were in orders of 10^{-5}–10^{-3} m^2 s^{-3} and 10^{-6}–10^{-4} m^2 s^{-3} at flow speeds <0.20 m s^{-1} for chromis and garden eel habitats, respectively. In the laboratory flume, with a grid 25 cm from the center, the dissipation rate increased 4–12 times compared to without the grid (Figure 3.2A,C).

Figure 3.3 shows the representative vertical velocity spectra obtained from ADV measurement in the field (chromis habitat) and PIV measurement in the flume (smooth bottom with the grid 35 cm upstream from the center). Two spectra overlap at >0.8 Hz at slow flow speed and at >2 Hz at middle flow speed, both of which correspond to an eddy size of about <1 cm, suggesting that the small-scale turbulence generated in the flume was comparable to that observed in the field. The same applied to the garden eel habitat. Comparing dissipation rates produced in the lab with those in natural habitats, the three levels of turbulence generated in the flume under 0.05 and 0.15 m s^{-1} represented weaker in situ levels for chromis, were comparable to in situ levels for garden eels under 0.05 m s^{-1}, and represented stronger in situ levels for the garden eels under 0.15 m s^{-1} (Figure 3.2B,D). Note that dissipation rates for weakest turbulence levels in the flume estimated from Eq. (3.7) may be overestimated because of the emphasized noise arising from numerical derivatives. Although the three levels of turbulence in the lab did not cover the full range in field habitats, they represented dissipation rates that fish experience in the field.

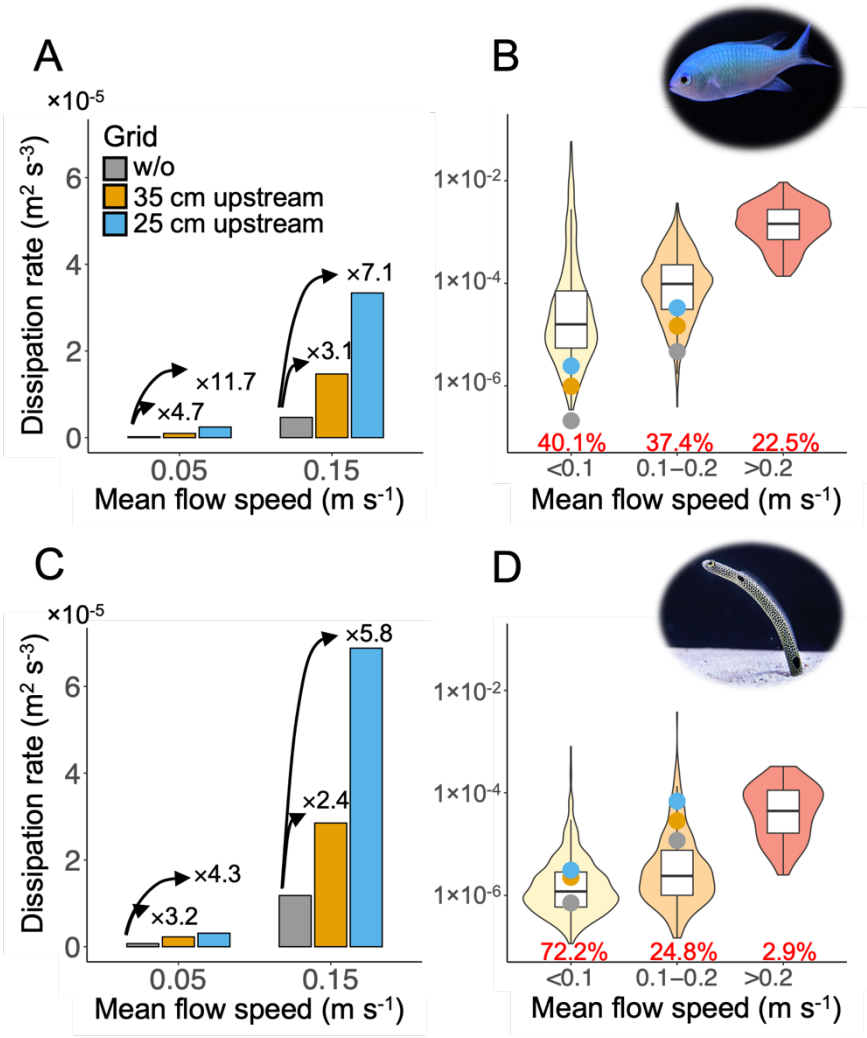

Figure 3.2. Dissipation rates enhanced by a static grid in the flume are comparable to those in fish habitats. (A,C) Bar plots of dissipation rates in the flume at different mean flow speeds and grid conditions with (A) a smooth bottom and (C) a sandy bottom. (B,D) Box plots of the dissipation rate in the (B) chromis habitat (n=1427) and (D) garden eel habitat (n=1493). Percentages in red show the percentages of time that each mean flow speed occurred. Points on box plots show dissipation rates produced in the flume.

Therefore, I defined these three levels as weak, medium, and strong turbulence levels and used them for foraging experiments. Reynolds stress and TKE in the flume and habitats were not comparable (Figure 3.4) probably because the strength in the energy-containing range is weak in the flume and there are errors derived from calculation of ADV data (Hansen and Reidenbach, 2017), but reported for reference.

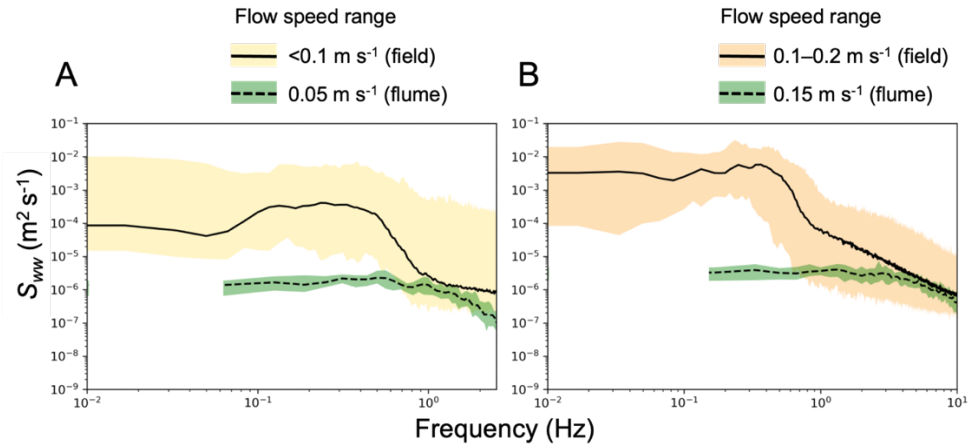

Figure 3.3. Small-scale turbulence was comparable in the flume and fish habitats. Vertical velocity spectra obtained from ADV in chromis habitat (yellow and orange shading) and from PIV in the flume with a grid 35 cm upstream on a smooth bottom (middle turbulence level; green shading) at (A) slow flow speed range and (B) middle flow speed range. Ranges of S_{ww} are shaded and the black lines are the medians at each frequency. The sample size was (A) 572 and (B) 534. Note that two spectra overlap at >0.8 Hz at slow flow speed range and at >2 Hz at middle flow speed range both of which correspond to eddy size of about <1 cm.

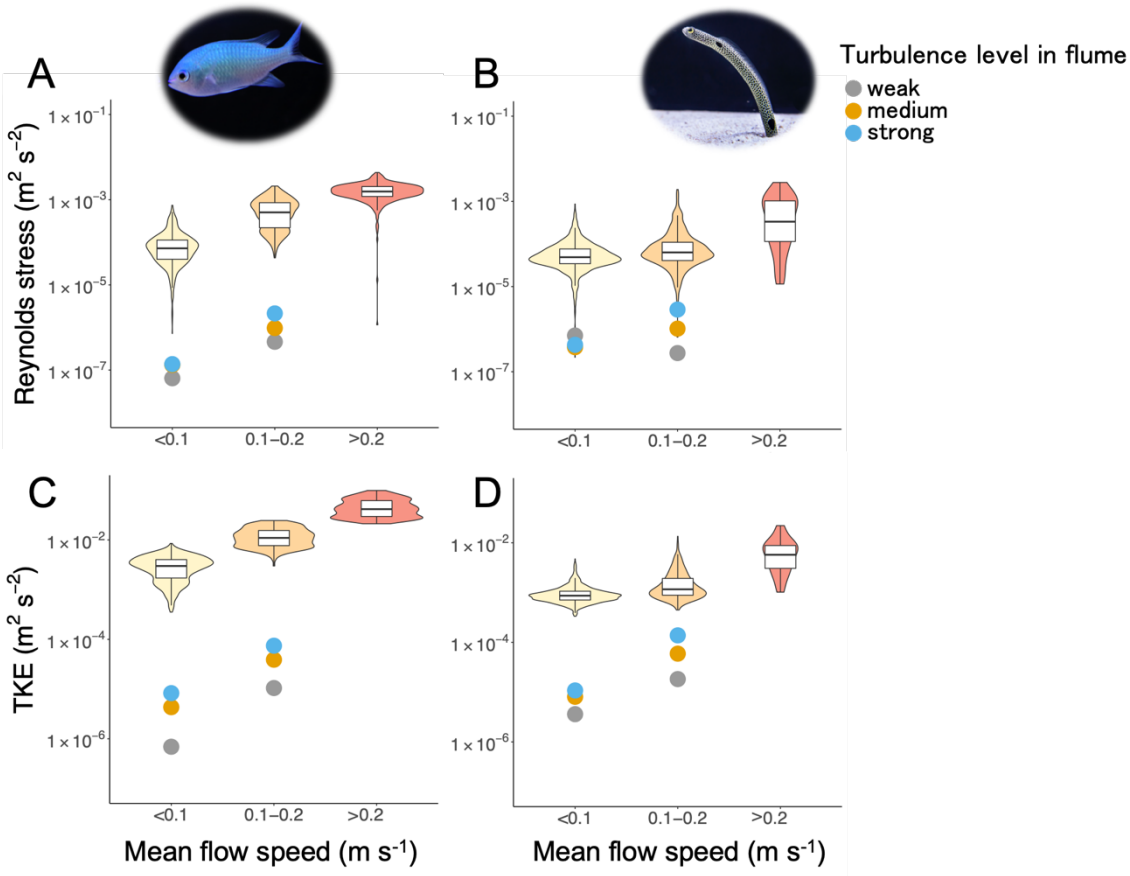

Figure 3.4. Reynolds stress and turbulence kinetic energy (TKE) enhanced by a static grid in the flume were compared to those in fish habitats. Box plots of the (A,B) Reynolds stress and (C,D) TKE in the (A,C) chromis habitat and (B,D) garden eel habitat. Filled circles show dissipation rates produced in the flume.

Effects of small-scale turbulence on feeding by chromis and garden eels

Chromis and garden eels showed different responses of feeding rate to changes in turbulence level. For chromis, feeding rates decreased significantly in strong turbulence at a flow speed of 0.05 m s^{-1} ($F_{(2,8)}$=6.92, p=0.02 in a mixed model), whereas they did not show any significant differences at a flow speed of 0.15 m s^{-1} ($F_{(2,8)}$=1.10, p=0.38 in a mixed model; Figure 3.4A). Chromis missed or gave up ≤5 times in the whole series of experiments, for a success rate of nearly 100% in every condition tested. For garden eels, feeding rates did not show significant differences at a flow speed of 0.05 m s^{-1} ($F_{(2,8)}$=0.57, p=0.57 in a mixed model), but they deceased in strong turbulence at a flow speed of 0.15 m s^{-1} ($F_{(2,8)}$=13.67, p<0.001 in a mixed model; Figure 3.5B). Garden eels did not show significant differences in success rate at a flow speed of 0.05 m s^{-1} ($F_{(2,8)}$=0.54, p=0.60 in a mixed model), but their success rate diminished significantly at stronger turbulence at a flow speed of 0.15 m s^{-1} ($F_{(2,8)}$=5.33, p=0.03 in a mixed model; Figure 3.6).

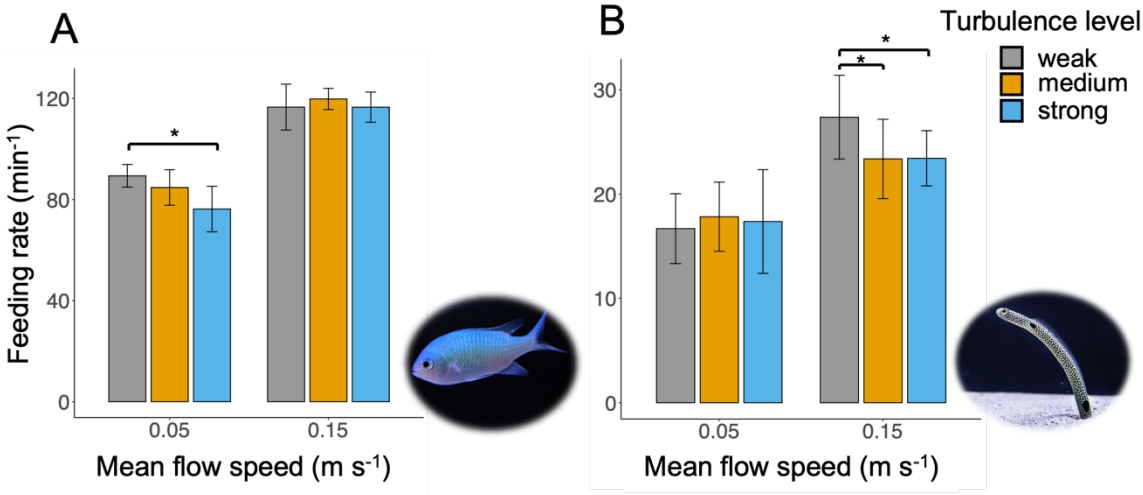

Figure 3.5. Stronger turbulence reduces feeding rates of (A) chromis at slower flow speed and (B) garden eels at faster flow speed. Values are means ±s.d. among individuals (n=5). Significance, adjusted with the Tukey post-hoc test, is indicated by asterisks (*p<0.05 in a mixed model).

To investigate effects of small-scale turbulence on foraging behavior, 3D-reconstructed behavior was examined. None of the foraging parameters (strike distance, strike time, strike speed, and reactive distance) showed significant responses to turbulence levels at either flow speeds for either fish (Figure 3.7; Table 3.1). Turbulence levels had no significant effect on the estimated energy expenditure of behavior (VeDBA) at either flow speed for either fish (Figure 3.7; Table 3.1). Eel body length outside the burrow was unaffected by turbulence levels (Figure 3.7; Table 3.1).

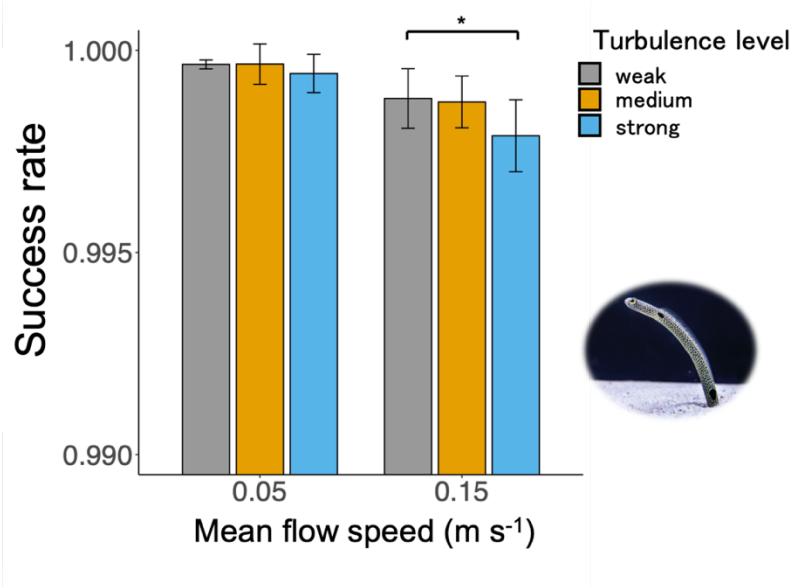

Figure 3.6. Feeding success rates of garden eels diminish at higher mean flow speeds and stronger turbulence. Values are means ±s.d. among individuals (*n*=5). Significance, adjusted with the Tukey post-hoc test, is indicated by asterisks (*p<0.05 in mixed model). Success rates of chromis were not plotted because of their nearly 100% success in every condition tested.

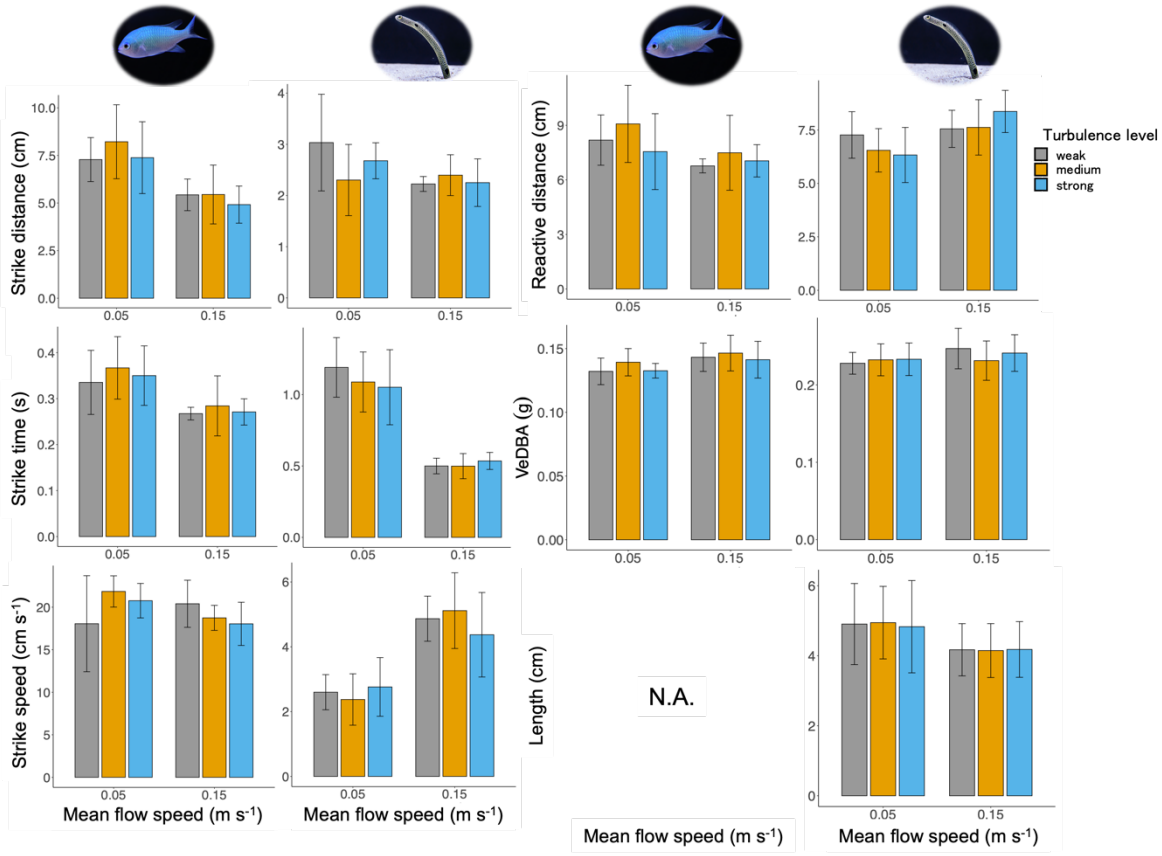

Figure 3.7. Foraging parameters, vectrial dynamic body acceleration (VeDBA), and eels' exposed body length are unaffected by turbulence levels. Values are means ±s.d. among individuals (*n*=5). Results of the mixed model ANOVA are provided in Table 3.1.

Table 3.1. Results of the mixed model ANOVA on foraging parameters, VeDBA, and body length outside the burrow. For all parameters, degrees of freedom in the numerator and denominator were 2 and 8, respectively.

Parameter	Fish species	Mean flow speed (m s^{-1})	*F*-value	*p*-value
Strike distance	Chromis	0.05	0.468	0.643
		0.15	0.550	0.598
	Garden eel	0.05	1.621	0.256
		0.15	0.417	0.673
Strike time	Chromis	0.05	0.340	0.722
		0.15	0.268	0.771
	Garden eel	0.05	2.152	0.179
		0.15	0.448	0.654
Strike speed	Chromis	0.05	1.689	0.244
		0.15	2.001	0.197
	Garden eel	0.05	0.443	0.657
		0.15	0.792	0.524
Reactive distance	Chromis	0.05	0.947	0.427
		0.15	0.418	0.672
	Garden eel	0.05	0.711	0.241
		0.15	0.899	0.445
VeDBA	Chromis	0.05	2.355	0.157
		0.15	0.913	0.440
	Garden eel	0.05	0.485	0.633
		0.15	4.000	0.063
Length outside	Garden eel	0.05	0.680	0.534
		0.15	0.088	0.917

To understand whether fish show different use of space depending on turbulence, space use in a 2D plane was examined. Chromis narrowed the space used in the *X*-*Y* plane at strong turbulence at a flow speed of 0.05 m s^{-1} ($F_{(2,8)}$=12.44, p<0.01 at 0.05 m s^{-1} and $F_{(2,8)}$=0.75, p=0.50 at 0.15 m s^{-1} in a mixed model; Figure 3.8A; 3.8). On the other hand, space use in the *X*-*Y* plane of garden eels was not affected by turbulence levels at either flow speed (Figure 3.8C). Turbulence levels did not significantly affect space use in the *X*-*Z* plane for either fish ($F_{(2,8)}$=1.78, p=0.23 at 0.05 m s^{-1} and $F_{(2,8)}$=1.86, p=0.22 at 0.15 m s^{-1} for chromis and $F_{(2,8)}$=0.86, p=0.46 at 0.05 m s^{-1} and $F_{(2,8)}$=0.75, p=0.50 at 0.15 m s^{-1} for garden eels; Figure 3.8B,D).

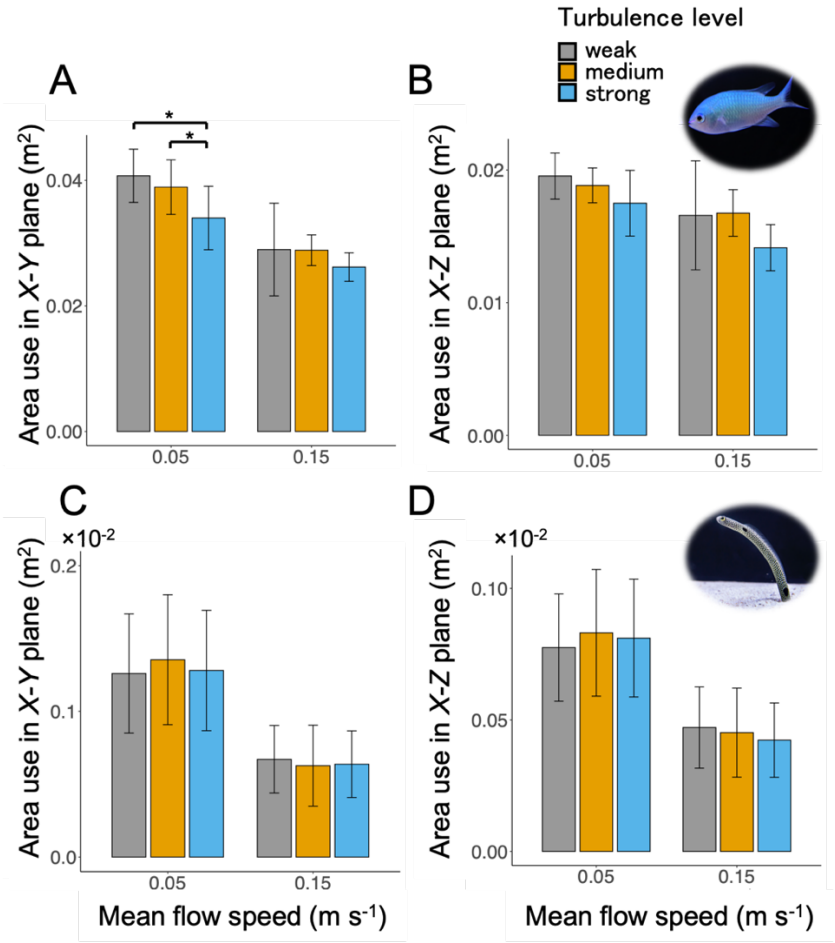

Figure 3.8. Stronger turbulence reduces area use in *X-Y* plane by (A) chromis (C) but has no significant effects on that by garden eels whereas (B,D) neither fish showed significant effects of turbulence on area use in *X-Z* plane. Values are means ±s.d. among individuals (n=5). Significance, adjusted with the Tukey post-hoc test is indicated by asterisks (*p<0.05 in a mixed model).

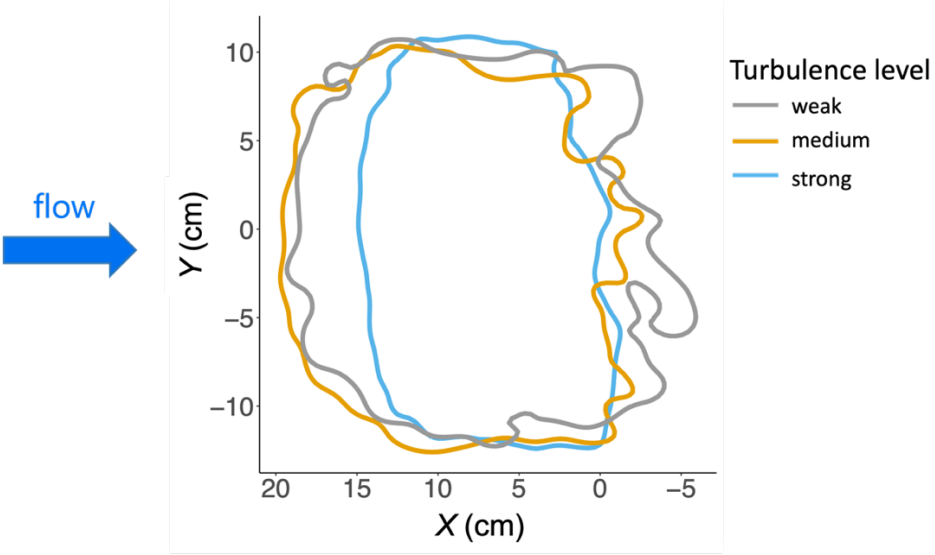

Figure 3.9. Area use of a representative chromis in top view at a flow speed of 0.05 m s^{-1} decreased and shifted downstream in the flume under strong turbulence.

3.4. Discussions

Flow conditions in the field

Chromis inhabit *Acropora* corals, forming schools at depths of ≤12 m (Randall, 1967). The surveyed habitat was about 3 m in depth and dominated by wave driven oscillatory flows. Turbulence in this environment is likely caused by bottom roughness and breaking surface waves. To describe turbulence levels, I reported dissipation rates because at plankton-length (millimeter) scale, turbulence behaves in an approximately isotropic manner and is controlled by local energy dissipation (Jiménez, 1997). As such, local values of the dissipation rate are an important parameter that controls the turbulence involved in the feeding of zooplanktivorous fish. The observations of dissipation rates are consistent with previous studies of shallow-reef lagoons dominated by oscillatory flows (Huang et al., 2012). The dissipation rates in oscillatory flows were higher than those measured for unidirectional flows at fringing coral reefs (Reidenbach et al., 2006a), suggesting that oscillatory flows enhance turbulence (Huang et al., 2012; Reidenbach et al., 2006b).

Garden eels live in sandy habitats, usually at the fringes of coral reefs at depths of 7–45 m (Castle and Randall, 1999). The surveyed habitat was 16 m deep and dominated by tidal water motion. The mean flow speed was relatively slow, where flow speed of ≤0.1 m s^{-1} occurred more than 70% of time. Turbulence there is probably produced mainly by the benthic boundary environment, with few patches of rocks, corals, and various animals. Observed dissipation rates of 10^{-6}–10^{-4} m^2 s^{-3} were comparable to observations on a sandy bottom in the Red Sea (Reidenbach et al., 2006a).

In terms of hydrodynamic conditions, there are two obvious differences between habitats of chromis and garden eels: bottom types and oscillation of flows. While chromis habitat comprises many patches of corals and rocks on the seafloor, garden eel habitat has tens of square meters of open, sandy flats with few corals or rocks. The drag coefficient of rough coral substrates is usually more than an order of magnitude larger than that of a sandy seabed, causing stronger mixing and mass transport (Monismith, 2007). Turbulent mixing between reef structure and the water column above contributes to replenishment of depleted plankton grazed by fish and corals; thus, it is thought to be a key feature to sustain biodiversity in reef communities (Genin et al., 2002; Monismith, 2007; Yahel et al., 2005). The complex geometry of corals provides this effective mass transport rate in addition to shelter for zooplanktivorous fish, such as chromis, enabling reefs to hold larger numbers and more species of fish. On the other hand, fish in sandy seabed experience less turbulent mixing and less available shelters, but higher availability of zooplankton because of fewer competitors (Yahel et al., 2005). Weaker Reynolds stresses observed in garden eel habitat also suggested weaker mixing (Figure 3.4). It is expected that dissipation rates are higher in environments with rougher coral bottoms compared to sandy seabed. However, Reidenbach et al (2006) found similar dissipation rates over corals and sandy bottoms at sites dominated by unidirectional flows, suggesting integrated effects of topography over large areas. In this respect, planktonic scale organisms, whose behavior depends on the dissipation rate, are expected to behave similarly over corals and sandy bottoms. In our study, we observed a 10-fold higher dissipation rate in chromis habitat which is likely caused by oscillatory flows. Oscillatory flow enhances dissipation rates in shallow lagoons (Huang et al., 2012). In this case, stronger background turbulence can affect plankton in various ways, such as by decreasing their awareness of predators (Gilbert and Buskey, 2005). Strong turbulent conditions under oscillatory flow, therefore, may be advantageous for fish that can manage the turbulence. Oscillatory flow also contributes to stronger mixing and penetrate more deeply into coral canopies (Lowe et al., 2008; Reidenbach et

al., 2007). Overall, clear differences in hydrodynamic conditions between chromis and garden eel habitats may highlight differences in adaptation strategies for each species.

Effects of small-scale turbulence on feeding

The dissipation rate produced in the flume mostly fell within the range of that in fish habitats, allowing me to run laboratory experiments that examined effects of small-scale turbulence with unidirectional flows that fish experience in their native habitats. Previous studies showed that flow speeds have significant effects on fish feeding. Mean flow speed that linearly increases the flux of prey increases feeding rate of fish until the flow severely affects predatory behavior (Ishikawa et al., 2022; Kiflawi and Genin, 1997). The novel method to quantify prey capture using high resolution videos enabled to find that the feeding rates of chromis and eels responded differently to small-scale turbulence. Chromis reduced their feeding rate in strong turbulence and slow flow speed, whereas eels reduced it at stronger turbulence and faster flow speed (Figure 3.5). Although the reason for these drops were originally expected to be the foraging behavior, foraging parameters did not show significant changes in response to turbulence levels tested in either chromis or eels (Table 3.1; Figure 3.7). For garden eels, the length of the body outside the burrow, which determines their feeding areas (Ishikawa et al., 2022), showed no significant changes (Table 3.1; Figure 3.7). These results corroborate a study of blennies, which found no effect of turbulent kinetic energy on their strike distance (Clarke et al., 2009). As shown in previous studies, these fish change their foraging parameters, such as strike distance and strike time to changes in mean flow speed to maintain feeding efficiency (Clarke et al., 2009; Ishikawa et al., 2022; Kiflawi and Genin, 1997). These results suggest that fish vary feeding movements with mean flow speed, and that these movements are insensitive to changes in small-scale turbulence at the levels tested. To estimate relative energy expenditure at different turbulence levels, I used the video-based VeDBA demonstrated in Chapter 2. Tested turbulence levels showed no effects on VeDBA of chromis or eels (Table 3.1; Figure 3.7). River fish reportedly reduce oxygen consumption under specific complex flows around bluff body (Taguchi and Liao, 2011). Grid-generated turbulence employed in our experiment is to avoid flows dominated by a specific frequency; thus, fish were not able to take advantage of those flow features that a bluff body produces by employing behaviors such as Karman-gaiting or entraining. Shiner perch reduce oxygen consumption at higher turbulence produced by a grid, possibly because they took advantage of high variability in turbulent energy with greater positional variability (van der Hoop et al., 2018). This theory does not apply to zooplanktivorous reef fish tested in this study because variability of area use did not increase with the turbulence level (Figure 3.8). Several other studies attribute higher oxygen consumption under stronger turbulence to changes in swimming kinematics and body destabilization (Enders et al., 2003; Maia et al., 2015). For turbulence to induce changes in swimming kinematics, the integral length scale needs to be large enough compared to the fish size (Lacey et al., 2012). The maximum integral length scale of the turbulence produced in this study was controlled by the grid size of 2 cm, which is smaller than two thirds of the body length of fish and may not be sufficient to affect swimming kinematics (Lacey et al., 2012; Lupandin, 2005). The small integral length scale may also explain unaffected VeDBA, regardless of changes in turbulence levels. Although VeDBA in this study was not correlated with quantified oxygen consumption, consistent VeDBA suggests that fish can maintain their energy consumption even under the strongest dissipation rate tested.

Chromis significantly decreased its area use and its feeding rate at slow flow speed and strong turbulence (Figure 3.5; 3.8). If the 17% decrease of the area use in the X-Y plane resulted mainly from a reduction in the streamwise direction (X), the time fish can spend

searching, striking, and capturing individual prey also decreased by 17%. This decrease closely matches the decrease in feeding rate of 15% and is especially significant at high prey density, because fish miss more prey items while attempting to capture one. Because chromis decreased the area they used by distancing themselves from the grid and moving to areas where turbulence intensity was weaker (Figure 3.9), free fish are thought to move to areas with weaker turbulence levels at slow flow speed. Schools of chromis changing locations were observed during a survey in the field. This behavior may be to choose favorable flow environments, although video recordings and multiple flow measurements are needed to confirm this. Although the reason that chromis did not show decreased feeding rate at the fast flow speed and stronger turbulence level tested is unclear, fast flows may not allow them to swim as freely as in slow flows.

In contrast, garden eels showed no significant effects of small-scale turbulence on their area use (Figure 3.8C,D). This reflects the unique lifestyle of garden eels with limited movement. Because garden eels do not swim to change feeding locations, they cannot change environments in which they feed as readily as freely swimming fish. Garden eels decreased their feeding rate at fast flow speed and stronger turbulence (Figure 3.5B) but showed no significant changes in movements at different turbulence levels (Table 3.1). The only significant difference was a decreased success rate in the same conditions, but this does not fully explain the decrease in feeding rate as the success rate was higher than 0.995 in all conditions (Figure 3.6). Based on the lack of apparent behavioral change and slight decrease in success rate, I suspect that garden eels took longer to decide to strike based on whether they can capture prey in stronger turbulence. The results likely overestimated their success rate in situ as most of their prey, such as copepods, have the ability to escape (Donham et al., 2017). Feeding on zooplankton with escape ability, they may need to carefully consider whether they can successfully capture the prey drifting toward them before striking, which is energetically expensive (Johansen et al., 2020). The lack of significant changes in success rate at slow flow speed implies that eels maintain their feeding rates regardless of the turbulence level tested. Fluctuation of prey movement is not a concern for eels at that flow speed.

Turbulence was expected to affect both prey movement and fish behavior. The small integral length scale and consistent foraging movements across ranges of dissipation rate tested suggests that the tested turbulence affects fish behavior by altering prey movement. Notably, the choice of dissipation rate as a representative turbulence parameter was therefore suitable in this regard, too. Free fish and anchored eels judged flows based upon movement of prey and adjusted their behavior in different ways. Freely swimming fish sought less turbulent areas and anchored eels spent more time searching.

Adaptation of fish to flow environments in their habitats

According to the field data, flow speeds in chromis habitat are faster than those of garden eel habitat. This difference in flows and results from the flume study suggest that their feeding behavior showed fit to flows that they experience most commonly. At faster flow speed, where chromis was able to maintain its feeding rate, the fish have adapted to capture the same amount of food, regardless of the turbulence level tested, whereas garden eels do not have this capacity, as they rarely experience the tested combination of fast flow speed and strong turbulence in their natural habitat. At slow flow speed, chromis avoided areas with strong turbulence, suggesting that they actively swim to find suitable flows for feeding. Because spatial flow patterns are highly heterogenous with complex shapes of corals and rocks (Asher and Shavit, 2019; Hench and Rosman, 2013), free fish may swim to find areas that are hydrodynamically appropriate for feeding. Anchored garden eels, on the other hand, must adapt to ambient flow; thus, they are able to maintain their feeding

rates over a wide range of turbulence levels at slow flow speed, which they experience most of the time in nature.

As discussed earlier, there are distinct hydrodynamic differences in driving flow and bottom type between habitats of chromis and garden eels. Chromis lives in a habitat with more replenishment of the food supply, greater spatial heterogeneity and shelter, but stronger turbulence, and more competitors and predators. Therefore, they have adapted to resist a wide range of turbulence levels at faster flow speeds and to swim to preferred flow habitat at slower flow speeds. Garden eels live in habitat with weaker turbulence, more food, fewer predators and competitors, but without shelter. Therefore, they acquired the ability to create a shelter and adapted to a wider range of turbulence levels at slower flow speeds.

3.5. Chapter Conclusion

By combining detailed flow measurement and turbulence analysis in the fish habitats and precise measurements of their feeding in a laboratory flume, this study indicates that the respective responses of freely-swimming fish, *Chromis viridis*, and anchored garden eels, *Heteroconger hassi*, to small-scale turbulent flows correspond well to the different flow environments prevailing in their respective habitats. These responses allow free-swimming fish to maintain high feeding rates under conditions of strong flows while anchored garden eels do so under conditions of weak flows. Turbulence effects of aquatic animals are often overlooked possibly because of the complexities in characterizing turbulence. However, as shown in this study, changes in small-scale turbulence affect feeding behavior of planktivorous fish, which may end up influencing the material cycling in coral reefs. Thus, it is worth investigating effects on wider variety of animals and different aspects (e.g., genetic or physiological aspects) in future studies.

Conclusion

Flows are a key environmental factor for behavior, ecology, and evolution of aquatic animals. Earlier studies have examined flow effects mainly on swimming fish, whereas anchored fish have been poorly studied. Also, effects of mean flow speed have been a primary focus to simplify hydrodynamic conditions, and those of turbulent fluctuation have yet to be explored. Thus, this thesis aimed to understand behavioral adaptation and energy cost-benefit by comparing site-attached free fish and anchored garden eels with a focus on effects of both mean flow speed and small-scale turbulent fluctuation.

In Chapter 1, I examined feeding responses of garden eels to mean flow speed to compare with the previously known responses of free-swimming fish. Garden eels showed their unique strategy of using their burrow and bending their body to keep feeding at fast flow speeds. Their foraging model was represented as a semi-circular feeding area, a radius of which is the body length outside the burrow, being distinct from the wedge-shaped foraging volume of site-attached free fish. These findings suggest that the unique lifestyle with the self-made burrows enabled garden eels to adapt to changes in flow speeds differently than free fish.

In Chapter 2, I investigated the energy cost and benefit of free damselfish and anchored garden eels as the cost and benefit of coral reef fish have been under-examined, regardless of the importance of habitat estimation and environmental assessment. The cost-benefit models of damselfish and garden eels indicated different energetically efficient ranges of flow speeds which correspond to the flow speed ranges at each habitat, suggesting that the balance between energy acquisition and expenditure based on flow speed is one of the key factors for habitat selection of coral reef fish. The findings provide insight into the adaptation and habitat distribution of planktivorous fish in coral reefs.

In Chapter 3, I investigated effects of small-scale turbulence on free damselfish and anchored garden eels as turbulence effects on fish feeding was expected to be critical and complex but yet to be understood. While strong turbulence caused a significant reduction in feeding rates of free-swimming damselfish under slow flows, anchored eels were affected at fast flows. The reduction was associated with a reduced area use for damselfish and an extended search time for garden eels. The observed difference between the two types of fish well corresponded with differences in their respective habitats, where faster flows and stronger turbulence occurred in the habitat of free-swimming fish than that of anchored garden eels. These responses help these fish maintain high feeding rates at each flow environment.

Through the study, novel techniques and approaches were necessary. For example, energy costs of small fish during free-ranging behaviors were challenging to estimate. Taking advantage of image processing techniques, such as automatic tracking of animal body features, I developed the video-based method for the energy cost estimation. Applying this method, I estimated energy costs of damselfish during feeding for the first time and found that feeding behavior costs approximately 3.8–6.8 times more than steady swimming. Also, turbulence levels in the laboratory were often inconsistent with those in the field according to previous studies. My research approach that combined flow measurements both in the laboratory and the fish habitats enabled detailed comparisons of the flows and provided a better understanding of flow characteristics that affect fish. These developments in methodology are also the main contributions of the field of study.

The findings of this study have led to more questions. For example, I used *Artemia* nauplii as a prey throughout the study because it drifts passively by flows and helps to avoid complexity from prey movements. However, planktivorous fish in coral reefs primarily feed on copepods with escape ability. Interaction between escaping prey and pursuing predators

in flows is an interesting research subject because turbulence can both help and interrupt zooplankton behavior. Also, the grid-generated turbulence in the flume did not reproduce the energy-containing range of turbulence in the fish habitats. Expected effects of turbulence on fish is at the centimeter-scale and is possibly more related to larger-scale turbulence than smaller-scale turbulence controlled in this study. Future studies need to address these points further to understand prey-predator interactions with turbulence effects.

In summary, this thesis demonstrated that feeding behavior and energy cost-benefit of planktivorous fish in coral reefs are adapted to flow environments in their habitats. Mean flow speed and turbulent fluctuation are both critical environmental factors controlling fish behavior and ecology. Comparison between site-attached free fish and anchored garden eels revealed feeding strategies specific to each foraging type. Investigation on effects of turbulent flows is still limited in terms of turbulence scales and species ranges. Continued study on turbulence effects on broader ranges of species would further advance our knowledge in ecology and evolution of fish.

References

Asaeda, T., Vu, T. K. and Manatunge, J. (2005). Effects of Flow Velocity on Feeding Behavior and Microhabitat Selection of the Stone Moroko Pseudorasbora parva : A Trade-Off between Feeding and Swimming Costs . *Trans. Am. Fish. Soc.* **134**, 537–547.

Asher, S. and Shavit, U. (2019). The Effect of Water Depth and Internal Geometry on the Turbulent Flow Inside a Coral Reef. *J. Geophys. Res. Ocean.* **124**, 3508–3522.

Avila, K., Moxey, D., de Lozar, A., Avila, M., Barkley, D. and Hof, B. (2011). The Onset of Turbulence in Pipe Flow. *Science (80-.).* **333**, 192–196.

Bates, D., Mächler, M., Bolker, B. and Walker, S. (2015). Fitting Linear Mixed-Effects Models Using lme4. *J. Stat. Softw.* **67**,.

Bidder, O. R., Goulding, C., Toledo, A., van Walsum, T. A., Siebert, U. and Halsey, L. G. (2017). Does the Treadmill Support Valid Energetics Estimates of Field Locomotion? *Integr. Comp. Biol.* **57**, 301–319.

Binning, S. A. and Roche, D. G. (2015). Water flow and fin shape polymorphism in coral reef fishes. **96**, 828–839.

Binning, S. A., Roche, D. G. and Fulton, C. J. (2014). Localised intraspecific variation in the swimming phenotype of a coral reef fish across different wave exposures. *Oecologia* **174**, 623–630.

Blake, R. W. (2004). Fish functional design and swimming performance. *J. Fish Biol.* **65**, 1193–1222.

Bricker, J. D. and Monismith, S. G. (2007). Spectral Wave–Turbulence Decomposition. *J. Atmos. Ocean. Technol.* **24**, 1479–1487.

Brownscombe, J. W., Lennox, R. J., Danylchuk, A. J. and Cooke, S. J. (2018). Estimating fish swimming metrics and metabolic rates with accelerometers: the influence of sampling frequency. *J. Fish Biol.* **93**, 207–214.

Butler, P. J., Green, J. A., Boyd, I. L. and Speakman, J. R. (2004). Measuring metabolic rate in the field: the pros and cons of the doubly labelled water and heart rate methods. *Funct. Ecol.* **18**, 168–183.

Castle, P. H. J. and Randall, J. E. (1999). Revision of Indo-Pacific Garden Eels (Congridae: Heterocongrinae), with descriptions of five new species. *Indo-Pacific Fishes* 1–52.

Chen, C.-T., Bănaru, D., Carlotti, F., Faucheux, M. and Harmelin-Vivien, M. (2019). Seasonal variation in biochemical and energy content of size-fractionated zooplankton in the Bay of Marseille (North-Western Mediterranean Sea). *J. Mar. Syst.* **199**, 103223.

Chow, V. T. (1959). *Open Channel Hydraulics*. McGraw-Hill College.

Clarke, R. D., Buskey, E. J. and Marsden, K. C. (2005). Effects of water motion and prey behavior on zooplankton capture by two coral reef fishes. *Mar. Biol.* **146**, 1145–1155.

Clarke, R. D., Finelli, C. M. and Buskey, E. J. (2009). Water flow controls distribution and feeding behavior of two co-occurring coral reef fishes: II. Laboratory experiments. *Coral Reefs* **28**, 475–488.

Depczynski, M. and Bellwood, D. (2005). Wave energy and spatial variability in community structure of small cryptic coral reef fishes. *Mar. Ecol. Prog. Ser.* **303**, 283–293.

Donham, E., Foster, M. S., Rice, M. R., Cailliet, G. M., Yoklavich, M. M. and Hamilton, S. L. (2017). Natural History Observations of Hawaiian Garden Eels, Gorgasia hawaiiensis (Congridae: Heterocongrinae), from the Island of Hawai'i.

Pacific Sci. **71**, 135–147.
Doron, P., Bertuccioli, L., Katz, J. and Osborn, T. R. (2001). Turbulence Characteristics and Dissipation Estimates in the Coastal Ocean Bottom Boundary Layer from PIV Data. *J. Phys. Oceanogr.* **31**, 2108–2134.
Elliott, J. M. and Davison, W. (1975). Energy equivalents of oxygen consumption in animal energetics. *Oecologia* **19**, 195–201.
Enders, E. C., Boisclair, D. and Roy, A. G. (2003). The effect of turbulence on the cost of swimming for juvenile Atlantic salmon (Salmo salar). *Can. J. Fish. Aquat. Sci.* **60**, 1149–1160.
Fausch, K. D. (1984). Profitable stream positions for salmonids: relating specific growth rate to net energy gain. *Can. J. Zool.* **62**, 441–451.
Finelli, C. M., Clarke, R. D., Robinson, H. E. and Buskey, E. J. (2009). Water flow controls distribution and feeding behavior of two co-occurring coral reef fishes: I. Field measurements. *Coral Reefs* **28**, 461–473.
Franks, P. J. S., Inman, B. G., MacKinnon, J. A., Alford, M. H. and Waterhouse, A. F. (2022). Oceanic turbulence from a planktonic perspective. *Limnol. Oceanogr.* **67**, 348–363.
Frappell, P. B., Blevin, H. A. and Baudinette, R. V. (1989). Understanding respirometry chambers: What goes in must come out. *J. Theor. Biol.* **138**, 479–494.
Fulton, C. J. and Bellwood, D. R. (2005). Wave-induced water motion and the functional implications for coral reef fish assemblages. *Limnol. Oceanogr.* **50**, 255–264.
Fulton, C. J., Bellwood, D. R. and Wainwright, P. C. (2005a). Wave energy and swimming performance shape coral reef fish assemblages. *Proc. R. Soc. B Biol. Sci.* **272**, 827–832.
Fulton, C. J., Bellwood, D. R. and Wainwright, P. C. (2005b). Wave energy and swimming performance shape coral reef fish assemblages. *Proc. R. Soc. B Biol. Sci.* **272**, 827–832.
Garde, B., Wilson, R. P., Fell, A., Cole, N., Tatayah, V., Holton, M. D., Rose, K. A. R., Metcalfe, R. S., Robotka, H., Wikelski, M., et al. (2022). Ecological inference using data from accelerometers needs careful protocols. *Methods Ecol. Evol.* **13**, 813–825.
Genin, A., Yahel, G., Reidenbach, M., Monismith, S. and Koseff, J. (2002). Intense Benthic Grazing on Phytoplankton in Coral Reefs Revealed Using the Control Volume Approach. *Oceanography* **15**, 90–96.
Gilbert, O. M. and Buskey, E. J. (2005). Turbulence decreases the hydrodynamic predator sensing ability of the calanoid copepod Acartia tonsa. *J. Plankton Res.* **27**, 1067–1071.
Gleiss, A. C., Dale, J. J., Holland, K. N. and Wilson, R. P. (2010). Accelerating estimates of activity-specific metabolic rate in fishes: Testing the applicability of acceleration data-loggers. *J. Exp. Mar. Bio. Ecol.* **385**, 85–91.
Gleiss, A. C., Wilson, R. P. and Shepard, E. L. C. (2011). Making overall dynamic body acceleration work: On the theory of acceleration as a proxy for energy expenditure. *Methods Ecol. Evol.* **2**, 23–33.
Grémillet, D., Lescroël, A., Ballard, G., Dugger, K. M., Massaro, M., Porzig, E. L. and Ainley, D. G. (2018). Energetic fitness: Field metabolic rates assessed via 3D accelerometry complement conventional fitness metrics. *Funct. Ecol.* **32**, 1203–1213.
Gross, T. F. and Nowell, A. R. M. (1983). Mean flow and turbulence scaling in a tidal boundary layer. *Cont. Shelf Res.* **2**, 109–126.
Halsey, L. G., Shepard, E. L. C., Quintana, F., Gomez Laich, A., Green, J. A. and Wilson, R. P. (2009). The relationship between oxygen consumption and body acceleration in a range of species. *Comp. Biochem. Physiol. Part A Mol. Integr.*

Physiol. **152**, 197–202.
Halsey, L. G., Shepard, E. L. C. and Wilson, R. P. (2011). Assessing the development and application of the accelerometry technique for estimating energy expenditure. *Comp. Biochem. Physiol. Part A Mol. Integr. Physiol.* **158**, 305–314.
Hamner, W. M., Jones, M. S., Carleton, J. H., Hauri, I. R. and Williams, D. M. (1988). Zooplankton, Planktivorous Fish, and Water Currents on a Windward Reef Face: Great Barrier Reef, Australia. *Bull. Mar. Sci.* **42**, 459–479.
Hansen, J. C. R. and Reidenbach, M. A. (2017). Turbulent mixing and fluid transport within Florida Bay seagrass meadows. *Adv. Water Resour.* **108**, 205–215.
Hartley, R. and Zisserman, A. (2004). Estimation – 2D Projective Transformations. In *Multiple View Geometry in Computer Vision*, pp. 87–131. Cambridge University Press.
Heatwole, S. J. and Fulton, C. J. (2013). Behavioural flexibility in reef fishes responding to a rapidly changing wave environment. *Mar. Biol.* **160**, 677–689.
Hedrick, T. L. (2008). Software techniques for two- and three-dimensional kinematic measurements of biological and biomimetic systems. *Bioinspiration and Biomimetics* **3**,.
Hench, J. L. and Rosman, J. H. (2013). Observations of spatial flow patterns at the coral colony scale on a shallow reef flat. *J. Geophys. Res. Ocean.* **118**, 1142–1156.
Hiatt, R. W. and Strasburg, D. W. (1960). Ecological Relationships of the Fish Fauna on Coral Reefs of the Marshall Islands. *Ecol. Monogr.* **30**, 65–127.
Higham, T. E., Stewart, W. J. and Wainwright, P. C. (2015). Turbulence, Temperature, and Turbidity: The Ecomechanics of Predator-Prey Interactions in Fishes. *Integr. Comp. Biol.* **55**, 6–20.
Hill, J. and Grossman, G. D. (1993). An Energetic Model of Microhabitat Use for Rainbow Trout and Rosyside Dace. *Ecology* **74**, 685–698.
Holzman, R., Reidenbach, M. A., Monismith, S. G., Koseff, J. R. and Genin, A. (2005). Near-bottom depletion of zooplankton over a coral reef II: relationships with zooplankton swimming ability. *Coral Reefs* **24**, 87–94.
Howard, E. W. and Bori, L. O. (1972). *Behavior of Marine Animals: Current Perspectives in Research*. Plenum Press, New York.
Huang, Z. C., Lenain, L., Melville, W. K., Middleton, J. H., Reineman, B., Statom, N. and McCabe, R. M. (2012). Dissipation of wave energy and turbulence in a shallow coral reef lagoon. *J. Geophys. Res. Ocean.* **117**, 1–18.
Ishikawa, K., Wu, H., Mitarai, S. and Genin, A. (2022). Effects of prey density and flow speed on plankton feeding by garden eels: a flume study. *J. Exp. Biol.* **225**, 1–10.
Jenkins, A. R. and Keeley, E. R. (2010). Bioenergetic assessment of habitat quality for stream-dwelling cutthroat trout (Oncorhynchus clarkii bouvieri) with implications for climate change and nutrient supplementation. *Can. J. Fish. Aquat. Sci.* **67**, 371–385.
Jiménez, J. (1997). Oceanic turbulence at millimeter scales. *Sci. Mar.* **61**, 47–56.
Johansen, J., Bellwood, D. and Fulton, C. (2008a). Coral reef fishes exploit flow refuges in high-flow habitats. *Mar. Ecol. Prog. Ser.* **360**, 219–226.
Johansen, J., Bellwood, D. and Fulton, C. (2008b). Coral reef fishes exploit flow refuges in high-flow habitats. *Mar. Ecol. Prog. Ser.* **360**, 219–226.
Johansen, J., Vaknin, R., Steffensen, J. and Domenici, P. (2010). Kinematics and energetic benefits of schooling in the labriform fish, striped surfperch Embiotoca lateralis. *Mar. Ecol. Prog. Ser.* **420**, 221–229.
Johansen, J. L., Akanyeti, O. and Liao, J. C. (2020). Oxygen consumption of drift-feeding rainbow trout: the energetic tradeoff between locomotion and feeding in flow. *J. Exp. Biol.* **223**, jeb220962.

Kenny, G. P., Notley, S. R. and Gagnon, D. (2017). Direct calorimetry: a brief historical review of its use in the study of human metabolism and thermoregulation. *Eur. J. Appl. Physiol.* **117**, 1765–1785.

Khrizman, A., Ribak, G., Churilov, D., Kolesnikov, I. and Genin, A. (2018). Life in the flow: unique adaptations for feeding on drifting zooplankton in garden eels. *J. Exp. Biol.* **221**,.

Kiflawi, M. and Genin, A. (1997). Prey flux manipulation and the feeding rates of reef-dwelling planktivorous fish. *Ecology* **78**, 1062–1077.

Kingsford, M. and MacDiarmid, A. (1988). Interrelations between planktivorous reef fish and zooplankton in temperate waters. *Mar. Ecol. Prog. Ser.* **48**, 103–117.

Korsmeyer, K. E., Steffensen, J. F. and Herskin, J. (2002). Energetics of median and paired fin swimming, body and caudal fin swimming, and gait transition in parrotfish (Scarus schlegeli) and triggerfish (Rhinecanthus aculeatus). *J. Exp. Biol.* **205**, 1253–1263.

Kuznetsova, A., Brockhoff, P. B. and Christensen, R. H. B. (2017). lmerTest Package: Tests in Linear Mixed Effects Models. *J. Stat. Softw.* **82**, 1–26.

Lacey, R. W. J., Neary, V. S., Liao, J. C., Enders, E. C. and Tritico, H. M. (2012). THE IPOS FRAMEWORK: LINKING FISH SWIMMING PERFORMANCE IN ALTERED FLOWS FROM LABORATORY EXPERIMENTS TO RIVERS. *River Res. Appl.* **28**, 429–443.

Lavoie, P., Djenidi, L. and Antonia, R. A. (2007). Effects of initial conditions in decaying turbulence generated by passive grids. *J. Fluid Mech.* **585**, 395–420.

Lear, K. O., Whitney, N. M., Brewster, L. R., Morris, J. J., Hueter, R. E. and Gleiss, A. C. (2016). Correlations of metabolic rate and body acceleration in three species of coastal sharks under contrasting temperature regimes. *J. Exp. Biol.* **220**, 397–407.

Lenth, R. V. (2016). Least-Squares Means: The R Package lsmeans. *J. Stat. Softw.* **69**,.

Liao, J. C. (2007). A review of fish swimming mechanics and behaviour in altered flows. *Philos. Trans. R. Soc. B Biol. Sci.* **362**, 1973–1993.

Lowe, R. J., Shavit, U., Falter, J. L., Koseff, J. R. and Monismith, S. G. (2008). Modeling flow in coral communities with and without waves: A synthesis of porous media and canopy flow approaches. *Limnol. Oceanogr.* **53**, 2668–2680.

Lupandin, A. I. (2005). Effect of Flow Turbulence on Swimming Speed of Fish. *Zoology* **32**, 558–565.

Lusk, G. (1932). Contributions to the Science of Nutrition: A Tribute to the Life and Work of Max Rubner. *Science (80-.).* **76**, 129–135.

Lyons, G. N., Halsey, L. G., Pope, E. C., Eddington, J. D. and Houghton, J. D. R. (2013). Energy expenditure during activity in the American lobster Homarus americanus: Correlations with body acceleration. *Comp. Biochem. Physiol. Part A Mol. Integr. Physiol.* **166**, 278–284.

Maia, A., Sheltzer, A. P. and Tytell, E. D. (2015). Streamwise vortices destabilize swimming bluegill sunfish (Lepomis macrochirus). *J. Exp. Biol.* **218**, 786–792.

Manatunge, J. and Asaeda, T. (1998). Optimal foraging as the criteria of prey selection by two centrarchid fishes. *Hydrobiologia* **391**, 223–240.

Marcoux, T. M. and Korsmeyer, K. E. (2019). Energetics and behavior of coral reef fishes during oscillatory swimming in a simulated wave surge. *J. Exp. Biol.* **222**,.

Mathis, A., Mamidanna, P., Cury, K. M., Abe, T., Murthy, V. N., Mathis, M. W. and Bethge, M. (2018). DeepLabCut: markerless pose estimation of user-defined body parts with deep learning. *Nat. Neurosci.* **21**, 1281–1289.

Metcalfe, J. D., Wright, S., Tudorache, C. and Wilson, R. P. (2016). Recent advances in telemetry for estimating the energy metabolism of wild fishes. *J. Fish Biol.* **88**, 284–

297.
Monismith, S. G. (2007). Hydrodynamics of Coral Reefs. *Annu. Rev. Fluid Mech.* **39**, 37–55.
Morgan, M. J. (1988). The influence of hunger, shoal size and predator presence on foraging in bluntnose minnows. *Anim. Behav.* **36**, 1317–1322.
Mtaweh, H., Tuira, L., Floh, A. A. and Parshuram, C. S. (2018). Indirect Calorimetry: History, Technology, and Application. *Front. Pediatr.* **6**, 1–8.
Nath, T., Mathis, A., Chen, A. C., Patel, A., Bethge, M. and Mathis, M. W. (2019). Using DeepLabCut for 3D markerless pose estimation across species and behaviors. *Nat. Protoc.* **14**, 2152–2176.
Nikora, V. I., Aberle, J., Biggs, B. J. F., Jowett, I. G. and Sykes, J. R. E. (2003). Effects of fish size, time-to-fatigue and turbulence on swimming performance: A case study of Galaxias maculatus. *J. Fish Biol.* **63**, 1365–1382.
Nilsson, G. E., Östlund-Nilsson, S. and Munday, P. L. (2010). Effects of elevated temperature on coral reef fishes: Loss of hypoxia tolerance and inability to acclimate. *Comp. Biochem. Physiol. - A Mol. Integr. Physiol.* **156**, 389–393.
Noda, M., Kawabata, K., Gushima, K. and Kakuda, S. (1992). importance of zooplankton patches in foraging ecology of the planktivorous reef fish Chromis chrysurus (Pomacentridae) at Kuchinoerabu Island, Japan. *Mar. Ecol. Prog. Ser.* **87**, 251–263.
Noda, T., Fujioka, K., Fukuda, H., Mitamura, H., Ichikawa, K. and Arai, N. (2016). The influence of body size on the intermittent locomotion of a pelagic schooling fish. *Proc. R. Soc. B Biol. Sci.* **283**, 20153019.
O'Brien, W. J., Barfield, M. and Sigler, K. (2001). The functional response of drift-feeding Arctic grayling: the effects of prey density, water velocity, and location efficiency. *Can. J. Fish. Aquat. Sci.* **58**, 1957–1963.
O'Gorman, E. J. and Hone, D. W. E. (2012). Body Size Distribution of the Dinosaurs. *PLoS One* **7**, e51925.
Olivieri, S., Viola, F., Mazzino, A. and Rosti, M. E. (2021). Direct numerical simulation of flapping flags in grid-induced turbulence. *Phys. Fluids* **33**, 085116.
Payne, N. L., Gillanders, B. M., Seymour, R. S., Webber, D. M., Snelling, E. P. and Semmens, J. M. (2011). Accelerometry estimates field metabolic rate in giant Australian cuttlefish Sepia apama during breeding. *J. Anim. Ecol.* **80**, 422–430.
Pearre Jr., S. (1980). The copepod width–weight relation and its utility in food chain research. *Can. J. Zool.* **58**, 1884–1891.
Pennycuick, C. J., Fast, P. L. F., Ballerstädt, N. and Rattenborg, N. (2012). The effect of an external transmitter on the drag coefficient of a bird's body, and hence on migration range, and energy reserves after migration. *J. Ornithol.* **153**, 633–644.
Peters, F. and Redondo, J. M. (1997). Turbulence generation and measurement: Application to studies on plankton. *Sci. Mar.* **61**, 205–228.
Piccolo, J. J., Hughes, N. F. and Bryant, M. D. (2008). Water velocity influences prey detection and capture by drift-feeding juvenile coho salmon (Oncorhynchus kisutch) and steelhead (Oncorhynchus mykiss irideus). *Can. J. Fish. Aquat. Sci.* **65**, 266–275.
Piccolo, J. J., Frank, B. M. and Hayes, J. W. (2014). Food and space revisited: The role of drift-feeding theory in predicting the distribution, growth, and abundance of stream salmonids. *Environ. Biol. Fishes* **97**, 475–488.
Pope, S. B. (2000). *Turbulent Flows*. Cambridge University Press.
Raffel, M., Willert, C. E., Wereley, S. T. and Kompenhans, J. (2007). *Particle Image Velocimetry*. Berlin, Heidelberg: Springer Berlin Heidelberg.
Randall, J. E. (1967). *Food Habits of Reef Fishes of the West Indies*.

Reidenbach, M. A., Monismith, S. G., Koseff, J. R., Yahel, G. and Genin, A. (2006a). Boundary layer turbulence and flow structure over a fringing coral reef. *Limnol. Oceanogr.* **51**, 1956–1968.

Reidenbach, M. A., Koseff, J. R., Monismith, S. G., Steinbuckc, J. V. and Genin, A. (2006b). The effects of waves and morphology on mass transfer within branched reef corals. *Limnol. Oceanogr.* **51**, 1134–1141.

Reidenbach, M. A., Koseff, J. R. and Monismith, S. G. (2007). Laboratory experiments of fine-scale mixing and mass transport within a coral canopy. *Phys. Fluids* **19**, 075107.

Rickel, S. and Genin, A. (2005). Twilight transitions in coral reef fish: The input of light-induced changes in foraging behaviour. *Anim. Behav.* **70**, 133–144.

Robson, A. A., Chauvaud, L., Wilson, R. P. and Halsey, L. G. (2012). Small actions, big costs: the behavioural energetics of a commercially important invertebrate. *J. R. Soc. Interface* **9**, 1486–1498.

Roche, D. G., Binning, S. A., Bosiger, Y., Johansen, J. L. and Rummer, J. L. (2013). Finding the best estimates of metabolic rates in a coral reef fish. *J. Exp. Biol.* **216**, 2103–2110.

Roche, D. G., Taylor, M. K., Binning, S. A., Johansen, J. L., Domenici, P. and Steffensen, J. F. (2014). Unsteady flow affects swimming energetics in a labriform fish (Cymatogaster aggregata). *J. Exp. Biol.* **217**, 414–422.

Rosenfeld, J. S. and Boss, S. (2001). Fitness consequences of habitat use for juvenile cutthroat trout: energetic costs and benefits in pools and riffles. *Can. J. Fish. Aquat. Sci.* **58**, 585–593.

Rotics, S., Kaatz, M., Resheff, Y. S., Turjeman, S. F., Zurell, D., Sapir, N., Eggers, U., Flack, A., Fiedler, W., Jeltsch, F., et al. (2016). The challenges of the first migration: movement and behaviour of juvenile vs. adult white storks with insights regarding juvenile mortality. *J. Anim. Ecol.* **85**, 938–947.

Saraux, C., Le Bohec, C., Durant, J. M., Viblanc, V. A., Gauthier-Clerc, M., Beaune, D., Park, Y.-H., Yoccoz, N. G., Stenseth, N. C. and Le Maho, Y. (2011). Reliability of flipper-banded penguins as indicators of climate change. *Nature* **469**, 203–206.

Schakmann, M. and Korsmeyer, K. E. (2023). Fish swimming mode and body morphology affect the energetics of swimming in a wave-surge water flow. *J. Exp. Biol.* **226**,.

Schlichting, H. and Gersten, K. (2017). *Boundary-Layer Theory*. 9th ed. Berlin, Heidelberg: Springer Berlin Heidelberg.

Shepard, E., Wilson, R., Halsey, L., Quintana, F., Gómez Laich, A., Gleiss, A., Liebsch, N., Myers, A. and Norman, B. (2008). Derivation of body motion via appropriate smoothing of acceleration data. *Aquat. Biol.* **4**, 235–241.

Silva, A. T., Santos, J. M., Ferreira, M. T., Pinheiro, A. N. and Katopodis, C. (2011). Effects of water velocity and turbulence on the behaviour of Iberian barbel (Luciobarbus bocagei, Steindachner 1864) in an experimental pool-type fishway. *River Res. Appl.* **27**, 360–373.

Speakman, J. R. and Racey, P. A. (1988). The doubly-labelled water technique for measurement of energy expenditure in free-living animals. *Sci. Prog.* **72**, 227–237.

Steffensen, J. F. (1989). Some errors in respirometry of aquatic breathers: How to avoid and correct for them. *Fish Physiol. Biochem.* **6**, 49–59.

Steffensen, J. ., Johansen, K. and Bushnell, P. . (1984). An automated swimming respirometer. *Comp. Biochem. Physiol. Part A Physiol.* **79**, 437–440.

Taguchi, M. and Liao, J. C. (2011). Rainbow trout consume less oxygen in turbulence:

the energetics of swimming behaviors at different speeds. *J. Exp. Biol.* **214**, 1428–1436.

Tang, M., Boisclair, D., Ménard, C. and Downing, J. A. (2000). Influence of body weight, swimming characteristics, and water temperature on the cost of swimming in brook trout (Salvelinus fontinalis). *Can. J. Fish. Aquat. Sci.* **57**, 1482–1488.

Theriault, D. H., Fuller, N. W., Jackson, B. E., Bluhm, E., Evangelista, D., Wu, Z., Betke, M. and Hedrick, T. L. (2014). A protocol and calibration method for accurate multi-camera field videography. *J. Exp. Biol.* **217**, 1843–1848.

Thielicke, W. (2014). The Flapping Flight of Birds.

Thielicke, W. and Sonntag, R. (2021). Particle Image Velocimetry for MATLAB: Accuracy and enhanced algorithms in PIVlab. *J. Open Res. Softw.* **9**, 12.

Thielicke, W. and Stamhuis, E. J. (2014). PIVlab – Towards User-friendly, Affordable and Accurate Digital Particle Image Velocimetry in MATLAB. *J. Open Res. Softw.* **2**,.

Trinci, G., Harvey, G. L., Henshaw, A. J., Bertoldi, W. and Hölker, F. (2017). Life in turbulent flows: interactions between hydrodynamics and aquatic organisms in rivers. *Wiley Interdiscip. Rev. Water* **4**, e1213.

Tritico, H. M. and Cotel, A. J. (2010). The effects of turbulent eddies on the stability and critical swimming speed of creek chub (Semotilus atromaculatus). *J. Exp. Biol.* **213**, 2284–2293.

Trudel, M. and Boisclair, D. (1996). Estimation of fish activity costs using underwater video cameras. *J. Fish Biol.* **48**, 40–53.

Tudorache, C., Jordan, A. D., Svendsen, J. C., Domenici, P., DeBoeck, G. and Steffensen, J. F. (2009). Pectoral fin beat frequency predicts oxygen consumption during spontaneous activity in a labriform swimming fish (Embiotoca lateralis). *Environ. Biol. Fishes* **84**, 121–127.

van der Hoop, J. M., Byron, M. L., Ozolina, K., Miller, D. L., Johansen, J. L., Domenici, P. and Steffensen, J. F. (2018). Turbulent flow reduces oxygen consumption in the labriform swimming shiner perch, Cymatogaster aggregata. *J. Exp. Biol.* **221**,.

Vandenabeele, S., Shepard, E., Grémillet, D., Butler, P., Martin, G. and Wilson, R. (2015). Are bio-telemetric devices a drag? Effects of external tags on the diving behaviour of great cormorants. *Mar. Ecol. Prog. Ser.* **519**, 239–249.

Watson, K. and Granger, R. (1998). Hydrodynamic effect of a satellite transmitter on a juvenile green turtle (Chelonia mydas). *J. Exp. Biol.* **201**, 2497–2505.

Webb, P. W. (1984). Body Form, Locomotion and Foraging in Aquatic Vertebrates. *Am. Zool.* **24**, 107–120.

Williams, T. M., Wolfe, L., Davis, T., Kendall, T., Richter, B., Wang, Y., Bryce, C., Elkaim, G. H. and Wilmers, C. C. (2014). Instantaneous energetics of puma kills reveal advantage of felid sneak attacks. *Science (80-.).* **346**, 81–85.

Wilson, R. P., White, C. R., Quintana, F., Halsey, L. G., Liebsch, N., Martin, G. R. and Butler, P. J. (2006). Moving towards acceleration for estimates of activity-specific metabolic rate in free-living animals: The case of the cormorant. *J. Anim. Ecol.* **75**, 1081–1090.

Wilson, A. M., Lowe, J. C., Roskilly, K., Hudson, P. E., Golabek, K. A. and McNutt, J. W. (2013). Locomotion dynamics of hunting in wild cheetahs. *Nature* **498**, 185–189.

Wilson, R. P., Börger, L., Holton, M. D., Scantlebury, D. M., Gómez-Laich, A., Quintana, F., Rosell, F., Graf, P. M., Williams, H., Gunner, R., et al. (2020). Estimates for energy expenditure in free-living animals using acceleration proxies: A

reappraisal. *J. Anim. Ecol.* **89**, 161–172.
Wright, S., Metcalfe, J., Hetherington, S. and Wilson, R. (2014). Estimating activity-specific energy expenditure in a teleost fish, using accelerometer loggers. *Mar. Ecol. Prog. Ser.* **496**, 19–32.
Yahel, R., Yahel, G. and Genin, A. (2005). Near-bottom depletion of zooplankton over coral reefs: I: diurnal dynamics and size distribution. *Coral Reefs* **24**, 75–85.